Touschek- and Gas Scattering Lifetime Investigations in the MAX IV 3 GeV Storage Ring

Jens Sundberg

Master's Thesis in Accelerator Physics
Master Program in Synchrotron Radiation Based Science
Faculty of Science
MAX-NFak

Supervisor: Åke Andersson

LUND UNIVERSITY

2017

to Hedvig

Acknowledgements

First, I want to express my gratitude to Åke Andersson for supervising me through this project, and for his support.

I would like to thank Anders Rosborg, Magnus Sjöström, Simon C. Leemann, Marek Grabski, Eshraq Al Dmour, David K. Olsson, Jonas Breunlin, Robin Svärd, Sara Thorin, Erik Mansten, Mikael Eriksson and Pedro Fernando Tavares. I want to give my special thanks to David Olsson and Mathias Brandin. I also want to thank all my family, and my friends.

Finally, I want to thank Malin Sallnäs, for making the writing of this thesis possible.

Jens Sundberg, May 2017

Abstract

The MAX IV 3 GeV storage ring is a fourth-generation electron synchrotron. At the time of writing in May 2017, it is the lowest emittance light source in the world. To study its performance is of foremost importance for the MAX IV Laboratory, its users and for upcoming synchrotrons. In this thesis, the MAX IV 3 GeV beam lifetime has been divided into its different components by experiments using in-vacuum copper blade scrapers. Touschek- and gas scattering lifetimes have been measured. The overall lattice momentum acceptance has been estimated by comparing measured Touschek scattering lifetimes with simulations. Observed and calculated current decays have been compared, based on a model using diverse types of decays for different lifetimes.

Abbreviations and Symbols

ID	insertion device
IR	infra-red
$LOCO$	linear optics from closed orbits
$MATLAB$	MathWorks matrix-based computational programming software
NEG	non-evaporable getter
OPA	magnet lattice design code
$Python$	programming language
RF	radio frequency
RGA	rest gas analyzer
UV	ultra-violet

α	momentum compaction factor
A	transversal acceptance
β	betatron function
β_v	velocity in terms of speed of light
$\bar{B}$	magnetic flux density vector
c	speed of light
C	storage ring circumference
d	limiting half-aperture distance
d_{scr}	scraper distance from beam center
e	elementary charge
ϵ_{acc}	overall momentum acceptance
$\epsilon_{acc,local}$	local momentum acceptance
$\epsilon_{lattice}$	lattice momentum acceptance
ϵ_{RF}	RF momentum acceptance
$\mathcal{E}$	emittance
η	dispersion function
E	nominal electron beam energy
f_{rev}	revolution frequency
f_{RF}	main RF frequency
f_s	synchrotron frequency
$\bar{F}$	force vector
γ	relativistic Lorentz factor
h	harmonic number
I	beam current

κ	emittance coupling factor
n_g	residual gas density
p	nominal electron beam momentum
ψ_s	synchronous phase
P	pressure
q	electron bunch charge
Q	betatron tune
r_e	classical electron radius
s	longitudinal coordinate
σ_E	rms beam energy spread
σ_s	longitudinal rms bunch length
$\sigma_{x,y}$	transversal rms beam size
σ'	transversal rms beam divergence
τ	beam lifetime
U_0	synchrotron radiation loss per turn
$\bar{v}$	velocity vector
V_{tot}	peak accelerating voltage
x	horizontal coordinate
y	vertical coordinate
Z	molecule atomic number

Contents

1. Introduction

The MAX IV Laboratory is a Swedish national synchrotron radiation research facility inaugurated in June 2016. At the time of writing in May 2017, the MAX IV Laboratory is the lowest emittance light source in the world. The facility contains a 300-meter-long 3.4 GeV linear electron accelerator, one 1.5 GeV- and one 3 GeV synchrotron radiation storage ring. The s-band linear accelerator is used as a full energy top-up injector for the two storage rings, and as a producer of femtosecond photon pulses for a short pulse facility realizing time-resolved scattering experiments. For both storage rings, there are currently 14 beamlines planned. At the beamlines, the intensive UV- and X-ray synchrotron radiation emitted from the storage rings is used for absorption, scattering and imaging experiments.

The aim with this master's thesis has been to obtain better understanding of the MAX IV 3 GeV electron beam lifetime. The beam lifetime determines at which pace the beam current decays, thus at which frequency new electrons need to be re-injected into the storage ring. To achieve this better understanding of the beam lifetime, the total lifetime of the electron beam needs to be divided into its different lifetime components. The different components of beam lifetime are mainly lifetimes due to elastic- and inelastic scattering on residual gas atoms, and Touschek-scattering lifetime due to collisions within an electron bunch. When the different lifetime components have been estimated, a model describing the storage ring current decay is compared to monitored current decays. The model is based on different lifetime components giving rise to diverse types of current decays.

Since the beam lifetime is determined by a vast number of parameters, studying the lifetime includes measuring transversal and longitudinal beam size, determining the quite inaccessible parameter momentum acceptance, measuring transversal acceptances and calculating the effective pressure seen by the electron beam. The pressure in the MAX IV 3 GeV storage ring is engaging since the storage ring is the first light source featured by a fully NEG-coated vacuum chamber system. NEG is short for non-evaporable getter and NEG coating supports the vacuum system in maintaining vacuum due to the surface being able to bind residual gas molecules.

The MAX IV 3 GeV storage ring is world leading in its performance considering emittance in electron synchrotrons. Studying the performance of the MAX IV 3 GeV storage ring is therefore of vast importance. The work carried out during, and in connection to, this master thesis project has been part of two conference proceedings [1, 2]. It will also be the main subject of a planned article to be posted to JSR, Journal of Synchrotron Radiation.

2. Theoretical background

In this section, the background theory needed for understanding the scope of this thesis is presented. Section 2.1 starts with an overview description of electron synchrotron storage rings, and is followed by characterizations of a few accelerator physics concepts. In section 2.2, beam lifetime is discussed in detail. Examples of detailed accelerator physics theory literature, recommended by the author, are works by Wiedemann [3] and Wille [4].

Section 2.1 contains introductory definitions in accelerator physics theory. If preferred, the reader can omit reading section 2.1 at this point, instead continue reading from section 2.2, and refer to section 2.1 when needed throughout the thesis.

2.1 Accelerator physics theory

2.1.1 Synchrotron storage rings

In an electron synchrotron storage ring, electrons circulate at high energies with velocities near the speed of light. The electrons are enclosed in vacuum chambers, which is needed to avoid collisions with gas particles. A synchrotron ring consists of straight sections and bends, and the electron beam is steered and focused using magnets. The arrangement of magnets around the ring, which is periodic, constitutes the storage ring magnet lattice. Several identical sections of magnets and straight sections, called achromats, shapes the periodic magnet lattice. Since electrons are charged particles, their velocity vector changes direction when they travel through a magnetic field, as a consequence of the Lorentz force acting upon them [4],

$$\overline{F} = e\,(\bar{v}\times\bar{B})\,, \tag{2.1}$$

where $\overline{F}$ is the Lorentz force, e the elementary charge, $\bar{v}$ the electron velocity and $\bar{B}$ is the magnetic flux density. As the direction of the velocity vector of a charged particle changes, the particle emits electromagnetic radiation in accordance with the Maxwell equations [3]. In synchrotrons, this electromagnetic radiation is highly intensive, focused and with energies in the infrared, visible, ultraviolet, soft- and hard X-ray regime. The purpose of synchrotron light sources is to use this radiation for scattering, imaging and absorption experiments. The synchrotron radiation is focused in extensions of the storage ring straight sections using X-ray optics. These extensions are called beamlines [5].

In the straight sections of third generation synchrotrons and later, insertion devices, ID's, are used to intensify the electromagnetic radiation emitted by the electrons [6]. The middle of a straight section is called a symmetry point, around which the magnet lattice is symmetric. There are mainly two types of insertion devices, undulators and wigglers. Both undulators and wigglers consist of arrays of magnet poles arranged in the electron velocity direction, the longitudinal

direction. This causes the electrons to wiggle round the straight orbit. Undulators and wigglers give different type of spectra of the emitted synchrotron radiation. For some insertion devices, it is also possible to control the light polarization.

Since the electrons emit synchrotron radiation, conservation of energy states that the electrons lose energy when circulating in the storage ring. This energy loss is compensated using radio frequency cavities. RF cavities are copper constructions supplied by an alternating radio frequency voltage which creates an oscillating electric field. As the electrons pass the cavity, the electric field recompense for the electron energy loss turn by turn. Due to the alternating voltage in the cavity, electron density of the beam in a synchrotron is not uniform, but the electrons in the beam are dived into bunches. The ring RF system frequency determines the distance between these electron bunches. The circumference of the storage ring then determines the number of bunches. The number of bunches is referred to as the harmonic number of the storage ring. As with ID's, RF cavities are situated in the storage ring straight sections.

2.1.2 Emittance

In a symmetry point, the emittance of an electron beam is the product of the electron beam size and divergence in one transversal plane,

$$\mathcal{E} = \sigma \cdot \sigma', \tag{2.2}$$

where $\mathcal{E}$ denotes the emittance, σ the beam size and σ' the beam divergence. The beam size is defined as one standard deviation of the Gaussian transverse charge distribution of the electron beam, for each transversal plane [4]. Beam size and divergence are measured in units of meter and radians respectively. The unit of emittance is therefore meter-radians. The emittance value is invariant for a non-accelerating beam, in accordance with Liouville's theorem [3].

There is also a single particle emittance. For an electron in a beam, illustrating a plot of electron angle x' versus position x in one transversal plane, at a specific longitudinal position s, creates an ellipse [4]. The area of this ellipse is constant with longitudinal position s, but the shape of the ellipse changes. The constant area of the ellipse portraits the invariance of the emittance parameter. The particle emittance is equal to this ellipse area divided by a factor of π. The x' versus x and y' versus y spaces are referred to as horizontal- and vertical phase-space respectively. A sketch of the phase-space ellipse is found in figure 2.1.

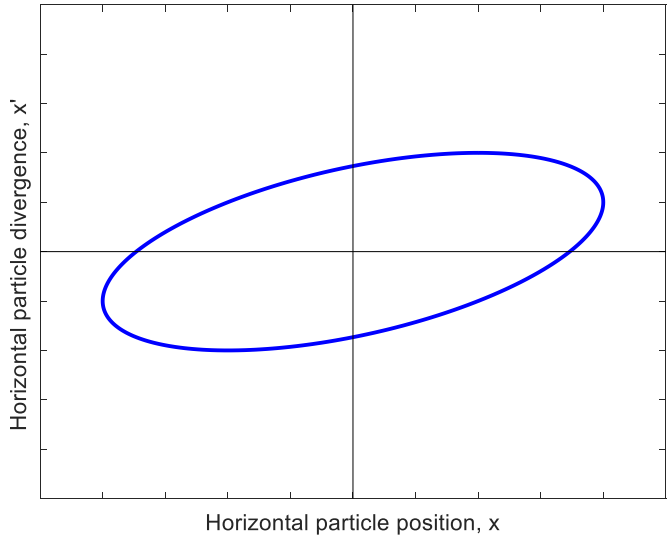

Figure 2.1 Horizontal plane phase-space ellipse. The particle divergence x' versus position x follows an ellipse trajectory. The particle emittance is invariant with longitudinal position s, and proportional to the ellipse area.

The beam emittances in the horizontal and vertical planes are related to each other via the emittance coupling factor [7], denoted by κ:

$$\kappa = \frac{\mathcal{E}_y}{\mathcal{E}_x}. \tag{2.3}$$

2.1.3 Betatron function and betatron tunes

The betatron function, short beta-function, is an amplitude function describing how the beam size varies with longitudinal s-position in each transversal plane. The beta-function is related to beam size and emittance through [4]:

$$\sigma = \sqrt{\mathcal{E} \cdot \beta}\,, \tag{2.4}$$

where σ denotes the beam size, $\mathcal{E}$ the emittance and β the beta-function. The beta-function is dependent on, and periodic with, the magnet lattice. It is therefore a function of the longitudinal position s in the storage ring. Combining equation (2.2) with equation (2.4) yields (in a symmetry point):

$$\beta = \frac{\sigma^2}{\mathcal{E}} = \frac{\sigma}{\sigma'}. \tag{2.5}$$

An electron circulating in a storage ring has always a certain deviation from nominal transversal x- and y-position, and nominal energy. Since the electron is steered and focused by magnets, these deviations cause the electron to oscillate around the ideal transversal orbit in the storage ring [4]. The number of transversal oscillations for one circumference length in each plane are called the horizontal and vertical betatron tunes of the synchrotron. The betatron tunes and their fractional parts are commonly denoted by Q_x, Q_y and q_x, q_y respectively. Figure 2.2 illustrates the horizontal and vertical betatron functions in the MAX IV 3 GeV storage ring. Betatron function values are according to design, with data imported from the lattice simulation tool OPA [8].

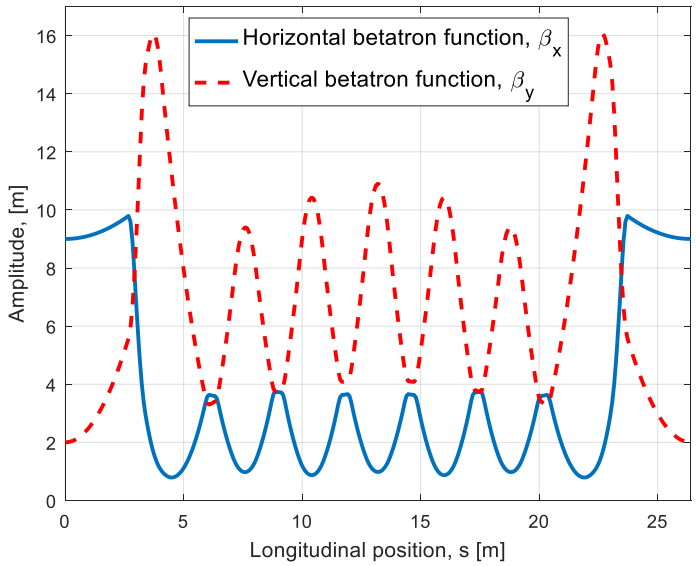

Figure 2.2 MAX IV 3 GeV storage ring design betatron functions. Horizontal and vertical betatron function amplitudes are plotted versus longitudinal position s in one of the 20 achromats (periodic magnet array sections) of the storage ring. The betatron functions are periodic with the achromats.

An important feature of the betatron function is its relation to the phase advance. Since the concept of phase advance is not used furthermore throughout this thesis, it is left as a reference [4].

2.1.4 Dispersion

The dispersion function, $\eta(s)$, describes how a certain electron energy deviation causes a transversal position deviation from the ideal orbit along the s-position in the storage ring, in one transversal plane. As with the betatron functions, the dispersion function is periodic with the magnet lattice and storage ring achromats. An electron with an energy deviation ΔE from the nominal energy E obtains a transverse horizontal x-position [4]:

$$x = x_0 + \eta_x \cdot \frac{\Delta E}{E}, \tag{2.6}$$

where x_0 is the nominal energy orbit x-position including the betatron oscillation, $\Delta E/E$ is the electrons relative energy deviation to the nominal electron energy E and η_x is the horizontal dispersion function. The horizontal size of the electron beam is affected by the dispersion by [4]:

$$\sigma_x = \sqrt{\mathcal{E}_x \cdot \beta_x + (\sigma_E \cdot \eta_x)^2}\,, \tag{2.7}$$

where σ_x is the horizontal beam size, $\mathcal{E}_x$ is the horizontal emittance, β_x is the horizontal beta-function, σ_E is the rms electron beam energy spread and η_x is the horizontal dispersion function. In a storage ring, an off-momentum particle follows the orbit given by the dispersion function, the dispersive orbit. Equations (2.6) and (2.7) are valid for the vertical plane as well, by exchanging x and y indexes. Generally, the vertical plane in a synchrotron has a dispersion which is zero or close to zero. Therefore, the vertical beam size is commonly described by equation (2.4).

2.1.5 Physical and dynamical acceptance

The acceptance is the maximum phase-space emittance that one single electron can have in a storage ring, defined for each transversal plane [4]. The acceptance is expressed [4, 9]:

$$A = \min\left(\frac{\left(d - \eta\frac{\Delta E}{E}\right)^2}{\beta}\right), \tag{2.8}$$

where A is the acceptance, d is the storage ring limiting half aperture and β is the betatron function. Commonly, acceptance refers to the on-momentum acceptance [9], given by $\Delta E/E = 0$. Furthermore, as mentioned in section 2.1.4, the vertical dispersion function equals zero, or close to zero, for most storage rings, yielding the same result for the vertical plane as the on-momentum case in the horizontal plane.

The acceptance is the minimum value of the physical acceptance and the dynamical acceptance of the storage ring. Physical acceptance refers to, for instance, vacuum chamber alignment, which physically limits the maximal phase-space emittance allowed for an electron in the storage ring. Dynamical acceptance means other effects than physical, such as magnetic field errors, which limit phase-space because of resonances, causing the electron to be lost from the stored beam.

2.1.6 Momentum acceptance

The local momentum acceptance, $\epsilon_{acc,local}$, which is a function of longitudinal position s, is the minimum value of the two parameters RF momentum acceptance and lattice momentum acceptance, described below [7].

The RF momentum acceptance, denoted by ϵ_{RF}, is the energy deviation allowed by the RF system in the storage ring. The total accelerating voltage gives rise to a maximum allowed energy deviation from the nominal energy for an electron to be part of the stored beam. The RF acceptance is constant for a given RF voltage, and can be expressed [7]:

$$\epsilon_{RF} = \sqrt{\frac{2\,U_0\,c}{\pi\,E\,\alpha\,C\,f_{RF}}\left(\cot\psi_s + \psi_s - \frac{\pi}{2}\right)}, \tag{2.9}$$

where U_0 is the synchrotron radiation losses per turn, f_{RF} is the RF frequency, E is the nominal energy, α is the momentum compaction factor, C is the storage ring circumference, c is the speed of light and ψ_s is the synchronous phase. The momentum compaction factor α is the fraction between relative circumference change and relative energy change, and depends on the storage ring magnet lattice. By equation (2.6), particles with different energies have different circumference lengths, and the momentum compaction factor describes how strong this effect is [5]:

$$\alpha = \frac{\frac{\Delta C}{C}}{\frac{\Delta p}{p}}. \tag{2.10}$$

The synchronous phase ψ_s is the phase that an electron with nominal energy has relative to the alternating RF voltage. Hence, the synchronous phase is the phase that provides an energy gain per turn equal to the synchrotron radiation losses per turn as the electron circulates in the storage ring.

The lattice momentum acceptance is the maximum energy deviation allowed for an electron to still be part of the beam, defined by the magnet lattice. The lattice momentum acceptance varies with longitudinal position s. Hence, the magnet lattice allows a beam electron to obtain different maximum energy deviations, depending on the s-position. This because the betatron oscillation induced by an energy deviation will attain different amplitudes depending on s-position. Furthermore, the dispersive orbit varies in amplitude with s-position. The lattice momentum acceptance is here denoted by $\epsilon_{lattice}$. The lattice momentum acceptance is not described mathematically in this thesis, since it demands deeper introduction in beam dynamics, but is studied empirically. The local momentum acceptance, which is a function of s, is expressed [7]:

$$\epsilon_{acc,local} = \min(\epsilon_{lattice}; \epsilon_{RF}). \tag{2.11}$$

The local momentum acceptance is for instance used when calculating Touschek-lifetime [10].

The overall momentum acceptance in a storage ring, denoted by ϵ_{acc}, is a measure of the averaged local momentum acceptance over all s-coordinates. Figure 2.3 illustrates the design

linear lattice momentum acceptance in the MAX IV 3 GeV storage ring, and the RF momentum acceptance for a total accelerating voltage of 1.08 MV.

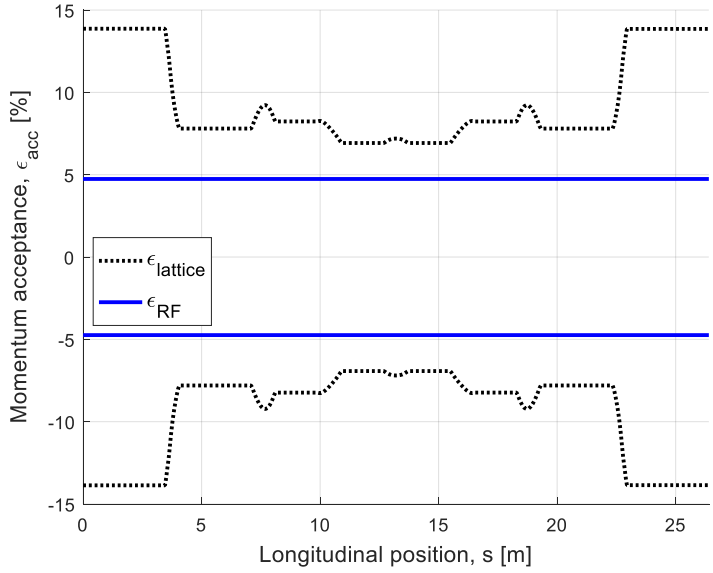

Figure 2.3 Design (linear) lattice momentum acceptance and RF momentum acceptance for a total accelerating voltage of 1.08 MV for one of the achromats in the MAX IV 3 GeV storage ring. The linear computation does not take higher order magnet field effects into account. Acceptances have been simulated in OPA [8].

2.1.7 Synchrotron oscillations

The RF system in a synchrotron storage ring recompense for the energy losses that the circulating beam electrons suffer each turn. The dominating energy losses of the beam electrons are losses due to synchrotron radiation. As mentioned in section 2.1.6, the synchronous phase ψ_s is the phase that an electron with nominal energy has relative the alternating RF voltage. The synchronous phase is determined by the ratio between synchrotron radiation losses and accelerating peak voltage in the RF cavities [3]:

$$\sin\psi_s = \frac{U_0}{V_{tot}}, \tag{2.12}$$

where ψ_s is the synchronous phase, U_0 is the synchrotron radiation loss per turn and V_{tot} is the peak accelerating voltage. Particles with lower energy than nominal will be bent more in the bending magnets compared to nominal, and will therefore travel at a shorter circumference. The opposite is valid for particles with higher energy than nominal. In an electron synchrotron, the synchronous phase is located at the slope with positive voltage and negative gradient of the RF wave. Since electrons with lower energy travel a shorter distance per turn, their energy gain will be higher than for an electron with nominal energy. The opposite is true for an electron with higher

energy than nominal. This system is self-regulating, and causes an oscillation of the electrons around the synchronous phase of the RF wave. This oscillation is called the synchrotron oscillation. The number of oscillations per turn in the storage ring is called the synchrotron tune, and the number of oscillations per second is called the synchrotron frequency. The oscillation is longitudinal spatially. Figure 2.4 illustrates the synchronous phase and synchrotron oscillation [3].

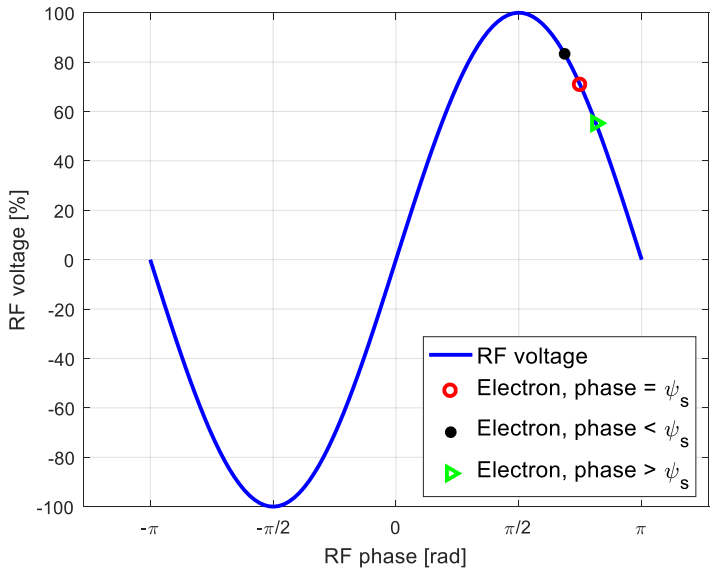

Figure 2.4 Synchronous phase and synchrotron oscillation. An electron with nominal energy arrives at the RF wave at the synchronous phase ψ_s. An electron with lower energy than nominal arrives earlier in phase and receives a higher energy gain, contrariwise for an electron with higher energy than nominal. All electrons oscillate around the synchronous phase. This oscillation is called the synchrotron oscillation.

The synchrotron frequency, and synchrotron tune, is related to the total accelerating voltage supplied in the RF cavities. The relation can be expressed [4]:

$$f_s^2 = f_{rev}^2 \frac{e\, V_{tot}\, h \cos\psi_s}{2\,\pi\,\beta_v^2\, E} \cdot \left(\alpha - \frac{1}{\gamma^2}\right), \tag{2.13}$$

where f_s is the synchrotron frequency, f_{rev} is the revolution frequency, e is the elementary charge, V_{tot} is the peak accelerating voltage, h is the harmonic number, ψ_s is the synchronous phase, β_v is the electron velocity in terms of the speed of light, E is the nominal energy, α is the momentum compaction factor and γ is the electron relativistic Lorentz factor.

2.2 Beam lifetime

This section characterizes decay processes, different storage ring beam lifetimes and how they constitute the total lifetime.

2.2.1 Decay processes and storage ring beam lifetime

Beam lifetime in a storage ring is a measure of the current loss over time. The lifetime, in its easiest approximation, is described by a pure exponential decay of beam current with time [4]:

$$I = I_0 \cdot e^{-\frac{t}{\tau_1}}, \tag{2.14}$$

where I is current at time t, I_0 is current at time $t = 0$ and τ_1 is the $1/e$–lifetime. Solving for τ_1 yields:

$$\tau_1 = -\frac{I}{\frac{dI}{dt}}. \tag{2.15}$$

Equation (2.15) is the instantaneous beam lifetime in a storage ring, and can be considered a definition for it. However, a more accurate description of the decrease of current with time than equation (2.14) is the combination of an exponential and a hyperbolic decay. This is explained by different particle loss processes. Loss processes which involve only one electron from the beam generates an exponential decay, but loss processes that involve two electrons from the beam engenders a hyperbolic decay [10]. The hyperbolic decay is written:

$$I = I_0 \cdot \frac{1}{1 + \frac{t}{\tau_2}}, \tag{2.16}$$

where τ_2 is the hyperbolic half-lifetime. Combining the two different decays yields for the total beam current decay with time [10],

$$I = I_0 \cdot \frac{e^{-\frac{t}{\tau_1}}}{1 + \left(1 - e^{-\frac{t}{\tau_1}}\right)\frac{\tau_1}{\tau_2}}. \tag{2.17}$$

Letting $\tau_2 \longrightarrow \infty$ in equation (2.17) gives the pure exponential decay by equation (2.14). Letting $\tau_1 \longrightarrow \infty$ in equation (2.17) gives the pure hyperbolic decay by equation (2.16). This can be shown by expanding e^{-t/τ_1} into a Taylor series:

$$I = I_0 \cdot \frac{\left(1 - \frac{t}{\tau_1} + \frac{t^2}{\tau_1^2} - \cdots\right)}{1 + \left(1 - \left(1 - \frac{t}{\tau_1} + \frac{t^2}{\tau_1^2} - \cdots\right)\right)\frac{\tau_1}{\tau_2}} \rightarrow I_0 \cdot \frac{1}{1 + \frac{t}{\tau_2}} \; as \; \tau_1 \rightarrow \infty. \tag{2.18}$$

An exponential, hyperbolic and a combined exponential and hyperbolic decay is illustrated in figure 2.5. A similar illustration has been made by Andersson and Streun [7].

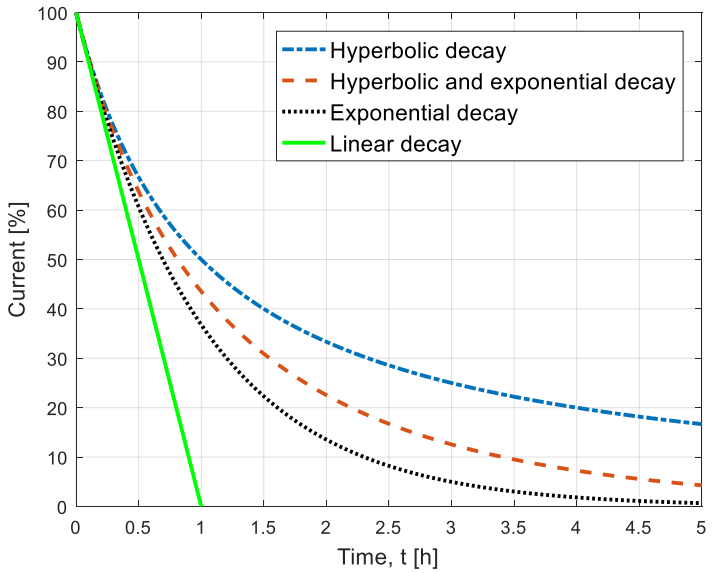

Figure 2.5 Hyperbolic, exponential, linear and combined hyperbolic and exponential decay processes. The exponential decay is illustrated for $\tau_1 = 1$ h, equation (2.14). The hyperbolic decay for $\tau_2 = 1$ h, equation (2.16). The combined exponential and hyperbolic decay for $\tau_1 = \tau_2 = 2$ h, equation (2.17). The linear decay illustrates $I = I_0 \cdot \left(1 - \frac{t}{\tau}\right)$ for $\tau = 1$ h. For all curves, $I_0 = 100\%$.

As seen in figure 2.5, all decay processes converge towards a linear decay as $t \rightarrow 0$. At most synchrotron laboratories, the lifetime is calculated over a time interval in the order of minutes or less. To calculate the instantaneous lifetime, a linear approximation is therefore sufficient.

Different lifetime components of the total lifetime can be described by different decay processes. Elastic scattering lifetimes, inelastic scattering lifetimes, Touschek lifetime and quantum lifetime are described in the following sections. The unit of lifetime is seconds, most often converted to hours. The naming convention for the separate lifetimes used in this thesis is similar to what is being used by Hansson [9].

2.2.2 Elastic scattering lifetime

Elastic scattering lifetime is a single particle loss effect due to the Coulomb force acting between electrons from the beam and residual gas molecules in the vacuum chamber. There are two types of elastic scattering, one on the nuclei and one on the electrons of the residual gas. In elastic scattering on nuclei, an electron is scattered by the Coulomb force when encountering a residual gas molecule nuclei. The electron is lost when it is scattered to a degree where its phase-space ellipse moves outside the acceptance of the machine.

Elastic scattering on nuclei can be expressed by [11]:

$$\frac{1}{\tau_{elastic\ nuclei}} = 3.217 \cdot 10^{22} \cdot \frac{2\,\pi\,c\,r_e^2\,Z^2\,\overline{\beta_y}\,P}{\gamma^2\,A_y}, \tag{2.19}$$

where $v \approx c$ is the electron velocity, r_e is the classical electron radius, Z is the average atomic number of the residual gas, $\overline{\beta_y}$ is the averaged vertical beta-function value over one circumference in the storage ring, P is the vacuum chamber pressure seen by the beam in units of [Torr], γ is the electron Lorentz factor and A_y is the vertical acceptance. The pressure P is related to the residual gas density by $n_g = 3.217 \cdot 10^{22} \cdot P$ [Torr], for an assumed residual gas temperature of 300 K. In equation (2.19) it is presumed that the electron loss is occurring in the vertical plane. For most electron storage rings, the vertical acceptance is smaller than the horizontal acceptance. This is due to the narrow vertical gaps needed by the insertion devices [9, 10]. In cases where the vertical acceptance is not much smaller than the horizontal acceptance, equation (2.19) needs to be modified by a factor. For a rectangular acceptance, this becomes: [9, 10, 12]

$$\frac{1}{\tau_{elastic\ nuclei}} = 3.217 \cdot 10^{22} \cdot \frac{2\,\pi\,c\,r_e^2\,Z^2\,\overline{\beta_y}\,P}{\gamma^2\,A_y} \cdot \frac{F(\rho)}{\pi}, \tag{2.20}$$

where $F(\rho)$ is given by [10]:

$$F(\rho) = \pi + (1+\rho^2) \cdot \sin(2\arctan\rho) + (2\rho^2 - 2) \cdot \arctan\rho\,. \tag{2.21}$$

The argument ρ is related to horizontal and vertical averaged beta-functions and acceptances [10]:

$$\rho = \sqrt{\frac{A_y}{A_x}\frac{\overline{\beta_x}}{\overline{\beta_y}}}\,. \tag{2.22}$$

We note that if $A_x \gg A_y$ then $\rho \approx 0$, $F(0) \approx \pi$, and equation (2.20) becomes identical to equation (2.19). When $\rho > 1$ in (2.22), equations (2.20) and (2.22) are valid by exchanging x and y indexes [9]. $A_y\,/\overline{\beta_y}$ is an approximation of the maximum allowed vertical scattering angle.

When the maximum allowed horizontal scattering angle is less than the vertical, hence $\rho > 1$ in equation (2.22), the indexes in equations (2.20) and (2.22) needs to be exchanged [9, 10].

When electrons from the beam instead scatter elastically against residual gas electrons, due to the Coulomb force, part of the kinetic energy can be transferred from the beam electron to the residual gas electron. The process is elastic since the total kinetic energy of the system is conserved. If the beam electron's relative energy deviation exceeds the momentum acceptance, the electron is lost from the beam. Elastic scattering on electrons can be expressed by [11]:

$$\frac{1}{\tau_{elastic\ electrons}} = 3.217 \cdot 10^{22} \cdot \frac{2\,\pi\,c\,r_e^2\,Z\,P}{\gamma\,\epsilon_{acc}}, \tag{2.23}$$

where ϵ_{acc} is the overall momentum acceptance.

2.2.3 Inelastic scattering lifetime

Inelastic scattering occurs when part of the kinetic energy of a beam electron is transferred into a photon in the scattering process. The kinetic energy of the system has changed and the scattering is inelastic. The energy of the beam electron changes and the particle is lost from the beam if the energy deviation is greater than the momentum acceptance [11]. There are two types of inelastic scattering, one on residual gas nuclei and one on electrons. Inelastic scattering lifetime is often referred to as bremsstrahlung lifetime [11]. Inelastic scattering is a single particle decay process, the decay becomes exponential.

Inelastic scattering on nuclei is expressed by [11]:

$$\frac{1}{\tau_{inelastic\ nuclei}} = 3.217 \cdot 10^{22} \cdot \frac{4\,c\,r_e^2\,Z^2 P}{137} \cdot \frac{4}{3} \cdot \left(\ln\frac{183}{Z^{\frac{1}{3}}}\right)\left(\ln\frac{1}{\epsilon_{acc}} - \frac{5}{8}\right). \tag{2.24}$$

Inelastic scattering on electrons is expressed by [9, 13]:

$$\frac{1}{\tau_{inelastic\ electrons}} = 3.217 \cdot 10^{22} \cdot \frac{4\,c\,r_e^2\,Z\,P}{137} \cdot \left(\ln\left(\frac{1194}{Z^{2/3}}\right) \cdot \frac{4}{3} \cdot \left(\ln\left(\frac{1}{\epsilon_{acc}}\right) - \frac{5}{8}\right) + \frac{1}{9} \cdot \left(\ln\left(\frac{1}{\epsilon_{acc}}\right) - 1\right)\right). \tag{2.25}$$

In literature, different notations are found for the gas scattering lifetimes. Equations (2.19) (2.23) and (2.24) are notations by Le Duff [11]. Equation (2.25) has been noted by Wrulich [13].

2.2.4 Touschek scattering lifetime

The Touschek scattering lifetime is a lifetime due to the Coulomb force acting between electrons within an electron bunch. As electrons oscillate around the ideal transversal orbit when they circulate in the storage ring, their different transversal velocities will lead to occasional interactions. Some of the transversal momentum is then transferred to the longitudinal momentum, and if the relative energy deviation exceeds the momentum acceptance of the storage ring, the two electrons from the bunch are lost [7, 11]. The Touschek lifetime is a two-particle process, the current decay becomes hyperbolic. The Touschek half-lifetime can be expressed [7]:

$$\frac{1}{\tau_{Touschek}} = \frac{r_e^2\, c\, q}{8\,\pi\, e\, \gamma^3\, \sigma_s} \cdot \frac{1}{C} \cdot \oint_C \frac{F\left(\left(\frac{\epsilon_{acc,local}(s)}{\gamma\, \sigma_{x\prime}(s)}\right)^2\right)}{\sigma_x(s)\, \sigma_y(s)\, \sigma_{x\prime}(s)\, \epsilon_{acc,local}(s)} ds \tag{2.26}$$

where r_e is the electron radius, $v \approx c$ is the electron velocity, q is the bunch charge, e is the elementary charge, γ is the electron Lorentz factor, σ_s is the bunch length, σ_x and σ_y are the transversal beam sizes, $\sigma_{x\prime}$ is the horizontal beam divergence at $x \approx 0$ and $\epsilon_{acc,local}$ is the local momentum acceptance. Transversal beam sizes, bunch length and divergence refer to rms values. The function $F(x)$ is given by [7]:

$$F(x) = \int_0^1 \left(\frac{1}{u} - \frac{1}{2} \cdot \ln\left(\frac{1}{u}\right) - 1\right) \cdot e^{-\frac{x}{u}}\, du \tag{2.27}$$

for $x \geq 0.01$, and

$$F(x) = \ln\frac{0.5772}{x} - \frac{3}{2} \tag{2.28}$$

for $x < 0.01$.

As expressed by Streun [7], the Touschek lifetime scales proportional to the rms bunch length σ_s, the square-root of the emittance coupling factor $\sqrt{\kappa}$ and the inverse of the bunch charge $1/q$. For a filling pattern in a storage ring where each electron bunch is evenly populated, the Touschek lifetime is inversely proportional to the beam current. Equations (2.26) – (2.28) are included to show the scaling probabilities of the Touschek scattering lifetime, and are used for Touschek lifetime calculations in the lattice simulation tool OPA [8].

2.2.5 Quantum lifetime

Electrons in a synchrotron beam has a transverse spatial distribution which is Gaussian. In theory, the tails of this Gaussian distribution are infinitely long [3, 9]. Because of the finite acceptance in a storage ring, the space that can be populated by the beam is limited and these tails are cut. Electrons circulating in a synchrotron emit radiation, and occasionally the electrons populating

the tails of the Gaussian distribution emit a high-energy photon and wander outside the acceptance of the storage ring due to the energy loss. This causes a decay of beam current with time. The lifetime of this decay is called the quantum lifetime. The quantum lifetime is generally very high compared to other lifetimes, and only impacts the current decay for small acceptances. A general rule for when the quantum lifetime is negligible is when the ratio between limiting half-aperture and beam size is seven or larger [9],

$$\frac{d_y}{\sigma_y} > 7\,. \tag{2.29}$$

This is generally true everywhere in a synchrotron in normal operation. The quantum lifetime is not described in further detail within thesis, it is considered infinite and is mentioned for the sake of completeness. The quantum lifetime is denoted:

$$\tau_{quantum}. \tag{2.30}$$

2.2.6 Total lifetime

The total lifetime is a combination of the different lifetimes mentioned in the previous subsections. It can be expressed by an inverse sum [10]:

$$\frac{1}{\tau_{total}} = \frac{1}{\tau_{elastic\ nuclei}} + \frac{1}{\tau_{elastic\ electrons}} + \frac{1}{\tau_{inelastic\ nuclei}} + \frac{1}{\tau_{inelastic\ electrons}} + \frac{1}{\tau_{Touschek}} + \frac{1}{\tau_{quantum}}. \tag{2.31}$$

The elastic scattering on nuclei and elastic scattering on electrons lifetimes can be expressed as one elastic lifetime:

$$\frac{1}{\tau_{elastic}} = \frac{1}{\tau_{elastic\ nuclei}} + \frac{1}{\tau_{elastic\ electrons}}. \tag{2.32}$$

Similarly, the inverse sum of the inelastic scattering lifetimes is commonly referred to as the inelastic-, or bremsstrahlung, lifetime:

$$\frac{1}{\tau_{inelastic}} = \frac{1}{\tau_{bs}} = \frac{1}{\tau_{inelastic\ nuclei}} + \frac{1}{\tau_{inelastic\ electrons}}. \tag{2.33}$$

Finally, the inverse sum of inelastic and elastic scattering lifetimes is named the gas scattering lifetime:

$$\frac{1}{\tau_{gas}} = \frac{1}{\tau_{elastic}} + \frac{1}{\tau_{inelastic}}. \tag{2.34}$$

3. MAX IV Laboratory

3.1 The Max IV 3 GeV Storage Ring

In this section, the lattice design and parameters of the MAX IV 3 GeV storage ring are summarized. The data in this section are found in the Lattice Design of the MAX IV Storage Rings [14] and The MAX IV storage ring project [15].

3.1.1 Magnet lattice

The MAX IV 3 GeV storage ring consists of 20 achromats. An achromat is an array of magnets and drift sections, symmetric with respect to its center. The achromats in the MAX IV 3 GeV storage ring are so-called multi bend achromats, consisting of 7 bending dipole magnets each. The 3 GeV storage ring is the first multi bend achromat storage ring taken into operation [14]. Apart from the bending dipole magnets, quadrupole-, sextupole- and octupole magnets are found within an achromat. The detailed beam optics of the MAX IV storage rings are beyond the scope of this thesis. A summary of the lattice characteristics is that the ultra-low horizontal emittance of the 3 GeV storage ring is a consequence of the low amplitude of the dispersion function, which in turn is a consequence of the small bending angle needed in each dipole magnet in a multi-bend achromat. The circumference of the 3 GeV storage ring is 528 m which gives an achromat length of 26.4 m. A sketch of the MAX IV 3 GeV storage ring achromat is found in figure 3.1.

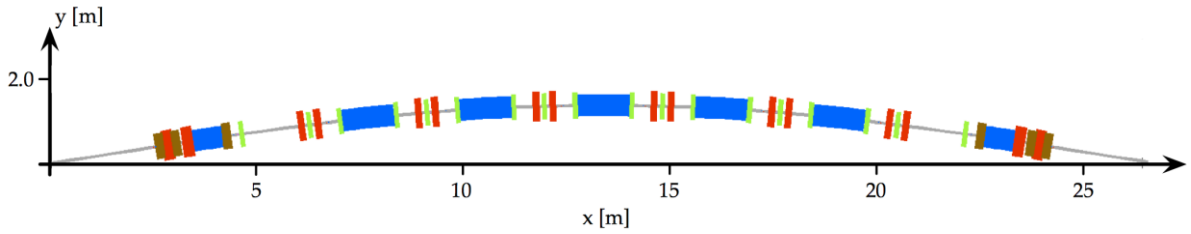

Figure 3.1 Sketch of the MAX IV 3 GeV storage ring achromat. Bending dipole magnets are indicated in blue, quadrupoles in red, sextupoles in green and octupoles in brown. The picture origin is the Lattice Design of the MAX IV Storage Rings [14].

3.1.2 RF system

The MAX IV 3 GeV storage ring is based on a 100 MHz radio frequency system. In total, 6 copper cavities are powered by 6 solid state transmitters with a future capability of supplying a maximum power of 120 kW each. The maximum power loss allowed in one cavity is 30 kW. As the electron beam current induces a decelerating field in the cavity, the so-called beam loading effect, the 120 kW power from each of the solid state transmitters is only needed at maximum beam current, 500mA, with all storage ring insertion devices installed. At the time of writing, in May 2017, the MAX IV 3 GeV storage ring has 5 RF cavities and transmitters in operation, with

the remaining sixth cavity in achromat 19 yet to be installed. The maximum stored beam current achieved so far in the 3 GeV storage ring is 200 mA.

3.1.3 Parameters

The MAX IV 3 GeV storage ring design parameters are found in table 3.1. Data is taken from the Lattice Design of the MAX IV storage rings [14]. Parameters not used or mentioned in this thesis has been omitted from the table. Bare lattice indicates that no insertion devices such as undulators or wigglers are accounted for.

Table 3.1 MAX IV 3 GeV storage ring design parameters. Parameters are found in the Lattice Design of the MAX IV storage rings [14].

Circumference	C	528	[m]
Number of achromats	-	20	-
Achromat length	-	26.4	[m]
Energy	E	3.0	[GeV]
Main RF frequency	f_{RF}	99.931	[MHz]
Harmonic number	h	176	-
Revolution frequency	f_{rev}	0.56779	[MHz]
Stored beam current	I	500	[mA]
Horizontal betatron tune	Q_x	42.20	-
Vertical betatron tune	Q_y	16.28	-
Horizontal emittance (bare lattice)	$\mathcal{E}_{\mathrm{x}}$	328	[pm rad]
Synchrotron radiation losses per turn (bare lattice)	U_0	363.8	[keV]
Energy spread (bare lattice)	σ_E	7.69×10^{-4}	-
Momentum compaction factor	α	3.06×10^{-4}	-
Required momentum acceptance	ϵ_{acc}	> 4.5%	-

4. Method

This section details the methods used throughout this thesis project. Section 4.1 gives a description of how primary storage ring parameters like current and accelerating voltage are measured. Section 4.2 characterizes transversal and longitudinal beam size measurements. Section 4.3 describes scraper measurements used to separate different lifetimes from the total lifetime, and details how scraper measurements are analyzed. Section 4.4 mentions the lattice simulation tool OPA [8].

4.1 Primary parameter measurements

4.1.1 Current and lifetime

A Bergoz NPCT device is used to measure the current of the MAX IV 3 GeV storage ring. NPCT is short for new parametric current transformer. An exponential fit to the current decay over time is made, and the instantaneous lifetime is calculated per equation (2.14). The lifetime calculation window is adjustable with a default setting of 60 seconds. As seen in figure 2.5, for small time intervals, a linear fit to the current decay with time is often sufficient to adequately determine the instantaneous lifetime.

4.1.2 Synchrotron frequency and accelerating voltage

The synchrotron frequency is measured with a spectrum analyzer. A storage ring BPM (beam position monitor) sum signal is connected to the spectrum analyzer and the electron beam longitudinal oscillations show up as side bands to the revolution frequency in the spectrum on the analyzer display. The synchrotron frequency is then given by the distance between these peaks and the revolution frequency harmonics. From the synchrotron frequency, the total accelerating voltage is calculated by equation (2.13). A stripline kicker is also connected to the spectrum analyzer. The stripline kicker is used to transversally shake the electron beam when measuring betatron tunes. A detailed description of the stripline kicker design can be found in references [16].

4.1.3 Betatron functions and dispersion function

Betatron functions have been determined by a MATLAB based LOCO [17]. LOCO is short for Linear Optics from Closed Orbits. LOCO measures a response matrix. From this response matrix quadrupole and skew quadrupole gradients are calculated [17]. The response matrix is a measurement of how the beam orbit is affected by a change in steering magnet strength, for each steering magnet in the storage ring. This determines the betatron functions for a given magnet lattice optics. In addition, a controlled RF frequency change is induced to determine the dispersion function. A detailed description of MATLAB based LOCO is found in references [17].

4.2 Beam sizes and emittance

The Touschek lifetime is proportional to the electron bunch volume by equation (2.26). Measuring the longitudinal size of the electron bunches, as well as the transversal beam size of the electron beam in both planes when studying the Touschek lifetime is therefore significant. Also, as illustrated by equation (2.7), the electron beam emittance can be determined by electron beam size, beam energy spread, dispersion- and betatron function at an s-position.

The longitudinal and transversal beam sizes are measured at an optical table located at a diagnostic beamline. At the diagnostic beamline, visible and near UV dipole emitted synchrotron light is used to measure longitudinal and transversal beam size. The emitted synchrotron light is focused, filtered and diffracted on the optical table. A description of the diagnostic beamline and optical table setup can be found in references [18, 19]. Sections 4.2.1 and 4.2.2 describe the methods for measuring the longitudinal and transversal beam sizes in the MAX IV 3 GeV storage ring.

4.2.1 Longitudinal bunch size measurements

The longitudinal size of the electron bunches is measured by dipole emitted synchrotron radiation light. The light is focused at the diagnostic beamline and guided onto a Hamamatsu OOS-01 sampling oscilloscope located at an optical table. The oscilloscope pictures the light pulse emitted from the electron bunch. This is done by sampling a certain bunch 2048 times with a well-controlled delay via a high-voltage sweep. Figure 4.1 illustrates a measurement of longitudinal bunch size. The image has been processed from a digital photo of the oscilloscope display.

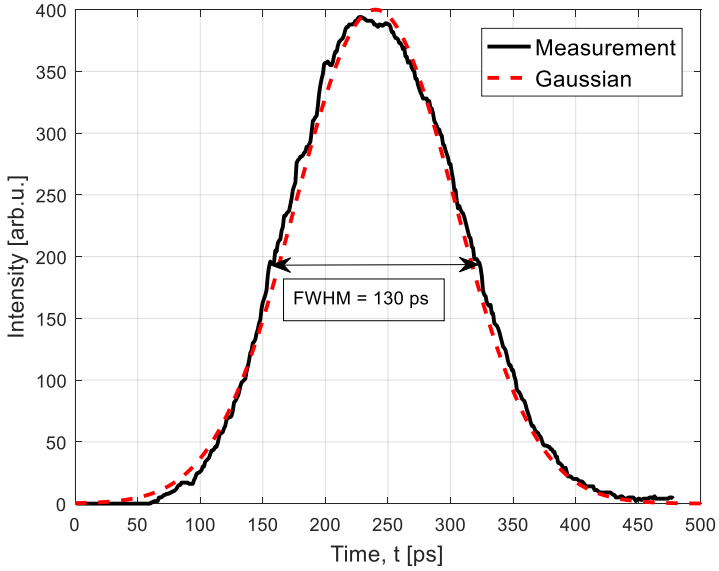

Figure 4.1 Longitudinal bunch size measurement in the MAX IV 3 GeV storage ring, at 70 mA stored beam current. The image has been processed from a digital photo of a Hamamatsu OOS-01 sampling-oscilloscope detecting emitted dipole synchrotron light. Measurement and a Gaussian function fit is shown to illustrate the intensity distribution.

Figure 4.1 illustrates that the intensity distribution of the emitted synchrotron light, i.e. the bunch electron density, follows a Gaussian distribution. The FWHM of the peak is measured and σ_s is calculated.

4.2.2 Transversal beam size and emittance measurements

The transversal beam size measurements are based on a technique using π- and σ-polarized synchrotron radiation light and a diffraction obstacle. The emitted synchrotron radiation is imaged by a CCD-camera. The maximum and minimum intensity ratio in the diffraction pattern is calculated by processing the image and the transversal beam size is evaluated [19]. Complete details about measuring the transversal beam size and calculating emittance in the MAX IV 3 GeV storage ring are described by Breunlin [18, 19].

Transversal beam sizes have been recorded simultaneously with scraper measurements. A MATLAB software tool for live monitoring the beam size and emittance has been developed by the author, using previous software developed by Breunlin [18]. The program measures the transversal beam sizes, illustrates the beam size variation with time in a graph and calculates the emittances in both planes according to equation (2.7). Simultaneously, time-stamped transversal beam size data is saved to a text file. Figure 4.2 illustrates the obstacle diffracted synchrotron radiation image recorded at the diagnostic beamline CCD camera.

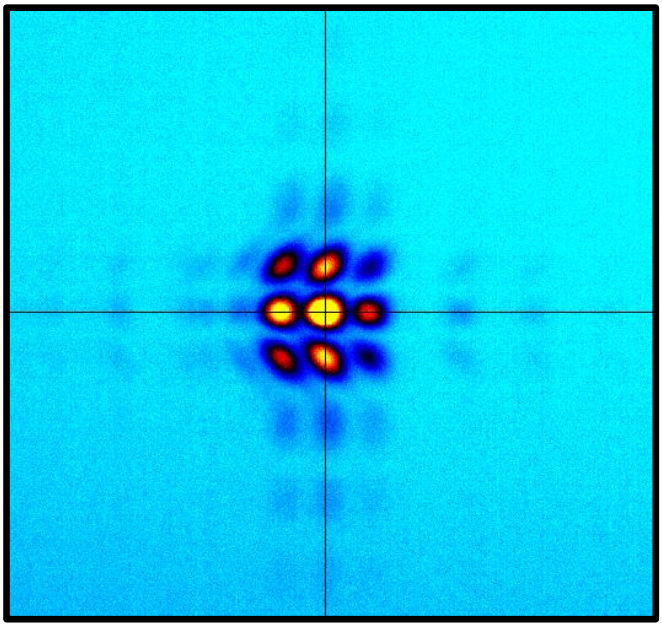

Figure 4.2 CCD camera picture from a MAX IV 3 GeV transversal beam size measurement. The dipole emitted synchrotron radiation is diffracted by an obstacle and the light is imaged. The measurement in the picture uses σ-polarized light in both transversal planes, and measures $\sigma_x = 20.73$ and $\sigma_y = 18.84$ µm at 70 mA current.

4.3 Scrapers

A scraper is a diagnostics tool used in synchrotron storage rings. The scraper is an in-vacuum copper blade which can be moved by a step motor, slightly past the center of the vacuum pipe. The MAX IV 3 GeV storage ring has four scrapers, two vertical and two horizontal. One of the horizontal scrapers are installed where the dispersion function equals zero, and one where it equals its maximum. At the time of writing, May 2017, the horizontal scraper at maximum dispersion has recently been put into operation. Horizontal scraper measurements during the work of this thesis have been made with the horizontal scraper located a zero-dispersion only. A drawing of the MAX IV 3 GeV vertical scrapers is shown in figure 4.3.

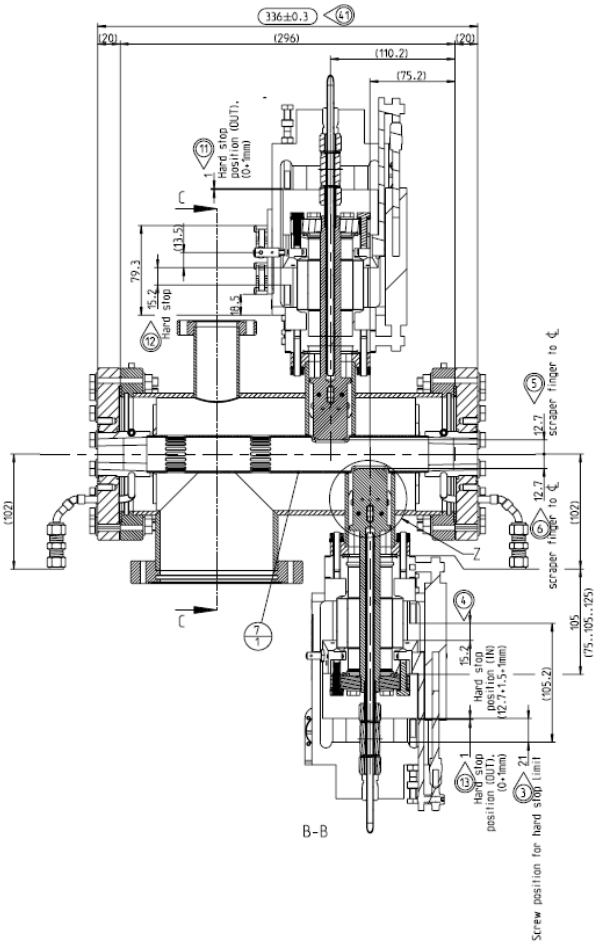

Figure 4.3 Drawing showing the inside side-view of the MAX IV 3 GeV storage ring vertical upper and vertical lower scrapers. Both scrapers are installed in the long straight section denoted by 301L, between achromats 20 and 01. The drawing has been provided to the author by the MAX IV Laboratory vacuum engineering unit.

4.3.1 Vertical scraper measurements

Vertical scraper measurements have been carried out to separate different lifetime components of the storage ring total lifetime. The scraper blade is moved from the outer position towards the beam center, while the total lifetime is being recorded. By equations (2.20), (2.23), (2.24), (2.25) and (2.26), the only lifetime component of the total lifetime that depends on the vertical aperture limitation, i.e. the vertical acceptance, is the elastic scattering on nuclei. By recording the total lifetime at each vertical scraper position while moving the scraper in steps towards the beam center, a fit can be made to the total lifetime as a function of scraper position. From the position where the scraper position starts having an impact on the total lifetime, the vertical acceptance and elastic scattering lifetime are both reduced as the vertical scraper is moved towards the beam center. The theoretic model predicts:

$$\tau_{total}\left(d_y^2\right) = \left(\frac{1}{\tau_{elastic\ nuclei}\left(d_y^2\right)} + \frac{1}{\tau_{other}}\right)^{-1}, \tag{4.1}$$

where τ_{other} is all the lifetimes, except for elastic scattering on nuclei, collected in one term:

$$\frac{1}{\tau_{other}} = \frac{1}{\tau_{elastic\ electrons}} + \frac{1}{\tau_{inelastic\ nuclei}} + \frac{1}{\tau_{inelastic\ electrons}} + \frac{1}{\tau_{Touschek}} + \frac{1}{\tau_{quantum}}. \quad (4.2)$$

The scraper position where the vertical scraper starts having an impact on the total lifetime gives an estimate of the vertical acceptance of the storage ring by equation (2.8). Since the lifetime is calculated by a NPCT device based on a 60 second time window, a 60 second delay is carried out at each scraper position before the total lifetime is recorded. The vertical scraper is moved in set-point steps of 200 μm. At the end of the scraper measurement, when the scraper reaches within approximately $7\sigma_y$ from the beam center, the quantum lifetime starts to have an impact on the total lifetime and the stored beam current decays rapidly. For measurements carried out during the work of this thesis, $7\sigma_y$ is approximately 130 μm, see results section 5.1.3. At the next scraper movement, the beam is lost and the measurement series is finished.

The scraper measurements performed during the work of this thesis project are automated by Python software, developed by the author. The scraper is moved in steps towards the beam center, with a 60 second delay between each step. The scraper position, storage ring current and storage ring total lifetime are recorded by 10 samples at a one second interval for each scraper position, until the scraper reaches the vicinity of the beam center and the beam is lost.

4.3.2 Analyzing vertical scraper measurements

In the data analysis of a vertical scraper measurement, a plot of total lifetime versus scraper distance from beam center is illustrated. A fit to the measurement data by equation (4.1) is made, and a numeric value of the elastic scattering lifetime on nuclei, as well as the term that summarizes all other lifetimes, is obtained. The model described by equation (4.1) includes the influence of d_y in the argument of the $F(\rho)$ factor in equation (2.20). The $F(\rho)$ factor is calculated separately, and included in the fit as a vector. The elastic scattering lifetime is a function of the vertical limiting aperture, and it can be computed for all aperture limitations. The analysis is done in MATLAB. Figure 4.4 shows an example of a vertical scraper measurement carried out at the MAX IV 3 GeV storage ring.

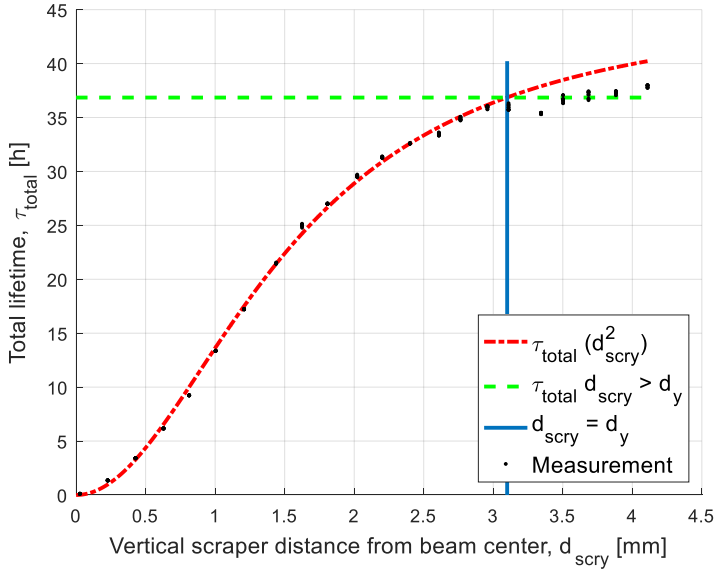

Figure 4.4 Example of a vertical scraper measurement in the MAX IV 3 GeV storage ring. The measurement was performed at 70 mA stored beam current. Black dots are total lifetime measurements, the red curve is the model fit by equation (4.1). The solid blue line indicates the position where the scraper starts affecting lifetime.

By equation (2.20), the elastic scattering lifetime on nuclei depends on the unknowns vertical and horizontal acceptance A_y and A_x, the squared atomic number of the residual gas Z^2, and the pressure seen by the electron beam P. The vertical scraper measurement yields the limiting vertical half-aperture at the position where the scraper starts affecting lifetime, indicated by the solid blue line in figure 4.4. The vertical acceptance is then calculated by equation (2.8), using measured values of the vertical betatron function. The horizontal acceptance is estimated by horizontal scraper measurements. The molecule values of the residual gas Z^2, Z, $Z^{2/3}$ and $Z^{1/3}$ are calculated from rest gas analyzer data. Rest gas analyzers detects the ratio of molecules with different mass in the residual gas. The rest gas analyzer data has been provided to the author by the vacuum engineering unit [20]. Once the Z^2 value of the residual gas has been evaluated, the pressure P becomes the only remaining unknown variable in equation (2.20), and can be calculated.

After a value for the pressure P has been obtained, the elastic scattering on electrons lifetime and the inelastic scattering lifetimes are calculated by equations (2.23), (2.24) and (2.25). The Touschek lifetime is determined by using equation (2.31) and letting the quantum lifetime be equal to infinity. This is allowed since the quantum lifetime only affects lifetime in the very last point of the scraper measurement. The value of the overall momentum acceptance ϵ_{acc} is obtained from comparing measured Touschek lifetimes with OPA lattice simulations [8]. By equation (2.26), the Touschek lifetime is dependent on the bunch volume. This motivates

recording the transversal beam size and longitudinal bunch length during scraper measurements, and allows comparison between measurements and OPA [8] simulations.

A vertical scraper measurement, combined with horizontal scraper measurements, rest gas analyzer data, betatron function measurements and an estimation of overall momentum acceptance is adequate for evaluating all separate lifetimes in a synchrotron storage ring. As a bi-product, transversal acceptances are determined. Scrapers are therefore powerful diagnostic tools used in synchrotrons.

4.3.3 Horizontal scraper measurements

Horizontal scraper measurements are carried out to estimate horizontal acceptance and to analyze the lifetime dependence on horizontal scraper position. A horizontal scraper measurement is performed the same way as a vertical scraper measurement. The storage ring total lifetime is recorded at each scraper position, and a plot of total lifetime versus scraper position distance from the beam center is made. Figure 4.5 illustrates a typical horizontal scraper measurement.

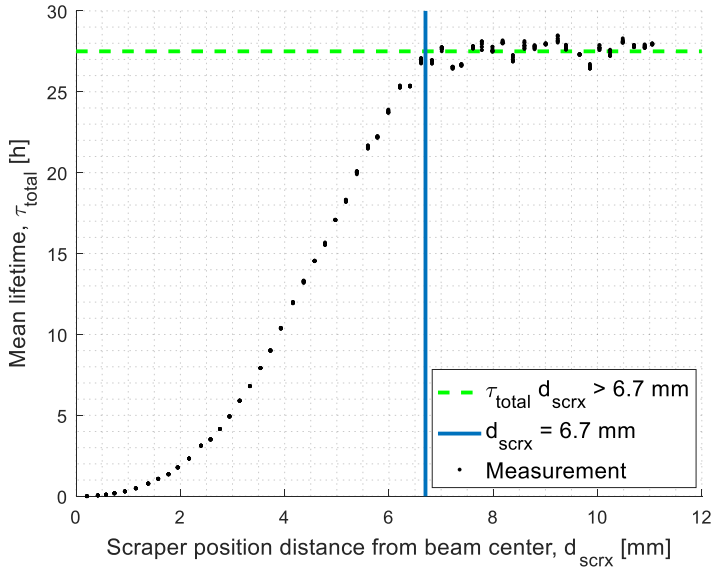

Figure 4.5 MAX IV 3 GeV storage ring horizontal scraper measurement. Since the horizontal scraper affects both horizontal acceptance and lattice momentum acceptance, the result from the horizontal scraper measurement is limited to a minimum value of the horizontal acceptance.

The horizontal acceptance is not as straight-forward to determine as the vertical acceptance. A Touschek-scattered off-momentum electron performs betatron oscillations around the dispersive orbit [7, 9]. This means that a Touschek-scattered electron will start oscillating horizontally around the dispersive orbit. The dispersive orbit also deviates horizontally from the ideal transversal orbit position. The dispersive orbit magnitude depends on the relative energy

deviation from nominal energy by equation (2.6). The limiting aperture caused by moving the horizontal scraper towards the beam center then affects both the maximum energy deviation allowed by the lattice, which can impact the Touschek lifetime, as well as the horizontal acceptance, which affects the elastic scattering on nuclei lifetime. The effect on total lifetime caused by lowered elastic scattering lifetime, due to decreased horizontal acceptance, can be small for cases when $A_x > A_y$. Therefore, the physical acceptance impact on the total lifetime can be hidden in the graph further out from the observed impact position, when illustrating a plot of total lifetime versus horizontal scraper position. However, since the maximum energy deviation allowed by the lattice is still limited by the physical and dynamical acceptance, the position where the scraper impacts the total lifetime in a lifetime versus horizontal scraper position curve will reveal a minimum value of the horizontal acceptance.

The dispersion function affects the total transversal deviation from the ideal orbit for an off-momentum electron. A horizontal scraper measurement with a scraper located at a zero-dispersion position therefore gives a better estimate of the horizontal acceptance than a measurement with a horizontal scraper located where the dispersion function is non-zero.

4.3.4 Combined vertical and horizontal scraper measurements

As described in section 4.3.3, Touschek-scattered electrons perform betatron oscillations around the dispersive orbit [7, 9]. In a storage ring with so-called betatron coupling, these horizontal betatron oscillations can couple to the vertical plane. This means that betatron coupling can cause Touschek-scattered electrons to be lost against the vertical scraper, during a vertical scraper measurement. The betatron coupling effect comes from sqew quadrupole- and displaced sextupole magnet fields [21].

A method to eliminate the possible Touschek-loss on the vertical scraper effect from betatron coupling is combining horizontal and vertical scrapers. By combining a vertical scraper measurement with a fixed horizontal scraper position inside the horizontal limiting aperture position, some Touschek-scattered electrons are lost against the horizontal aperture limited by the horizontal scraper, before being able to couple to the vertical plane and be lost against the vertical scraper. This decreases the possible effect that the vertical scraper has on the Touschek lifetime. Here, the influence of the $F(\rho)$ factor is decisive, and cannot be omitted. The $F(\rho)$ function might be omitted when $A_x \gg A_y$, which is often true during a vertical scraper measurement, with the horizontal scraper in its outer position. Vertical scraper scans for different horizontal scraper positions yield the elastic scattering on nuclei lifetime as a function of the horizontal scraper. By comparing simulations of the elastic scattering on nuclei lifetime with measurements, an estimation of the elastic scattering on nuclei lifetime can be withheld, which presumably is more accurate than the value obtained from a vertical scraper measurement only.

4.4 OPA lattice simulations

4.4.1 OPA lattice simulation software

The lattice simulation tool OPA, developed by Streun [8], has been used to simulate expected Touschek-lifetimes of the MAX IV 3 GeV storage ring. Input parameters needed for the simulation is the total accelerating voltage, stored beam current, longitudinal beam size and the emittance coupling factor. The simulation is made for the most updated storage ring design lattice per May 2017, 20121107v.430.

OPA computes Touschek lifetimes for natural bunch length. To compare simulated Touschek lifetimes in OPA with measurements, the natural bunch length used in OPA needs to be scaled against the measured bunch length. By simulating Touschek lifetimes that agree with measurements, the overall momentum acceptance can be estimated. Total accelerating voltage, stored beam current, longitudinal bunch size and the emittance coupling factor are determined by measurements.

5. Results

For the MAX IV 3 GeV storage ring, the different lifetimes have been separated from the total lifetime by analysis of scraper measurements. In addition to the vertical scraper measurements, horizontal scraper measurements, data from LOCO computations and rest gas analyzer data have been used to calculate the different lifetime components. Horizontal and vertical acceptances have been measured. A fitted model based on the lifetime component results has been made and compared to observed current decays. The pressure seen by the electron beam has been estimated. Simulations in the lattice simulation tool OPA have calculated the overall momentum acceptance parameter.

By combining horizontal and vertical scrapers while measuring lifetime, the estimation of the elastic scattering on nuclei lifetime was improved. The combined horizontal and vertical scraper measurements eliminate possible betatron-coupled Touschek scattered electrons being lost against the vertical scraper.

5.1 Residual gas, betatron functions and beam sizes

5.1.1 Residual gas

Residual gas analyzer data has been provided to the author by the MAX IV Laboratory vacuum engineering unit [20]. Calculations have been made to evaluate the values of the residual gas $Z^2, Z, Z^{2/3}$ and $Z^{1/3}$, where Z is the molecule atomic number. Linear approximations of the molecule Z-dependencies with stored beam current have been made. Tables 5.1 and 5.2 show summarized results from calculations using the residual gas analyzer data. The values of the molecule residual gas atomic number are used when calculating gas lifetimes and pressure seen by the electron beam.

Table 5.1 MAX IV 3 GeV storage ring residual gas data. The table shows the ratios of the three most common molecules detected using residual gas analyzers.

Date	Dose [Ah]	Current [mA]	H_2	CO	CH_4	$Other$
2017-01-26	130	42	96.6%	2.05%	0.59%	0.76%
2017-01-29	130	0	98.5%	0.69%	0.39%	0.42%

It is known from storage ring vacuum theory that the contributions to mass 28 from N_2 and to mass 16 from O^+ are negligible [21].

Table 5.2 MAX IV 3 GeV storage ring residual gas molecule atomic number calculations. The molecule values of $Z^2, Z, Z^{2/3}$ and $Z^{1/3}$ are calculated based on residual gas analyzer data.

Date	Dose [Ah]	Current [mA]	Z^2	Z	$Z^{2/3}$	$Z^{1/3}$
2017-01-26	130	42	4.60	2.35	2.17	2.07
2017-01-29	130	0	2.98	2.14	2.07	2.03

Using calculated atomic number values in table 5.2, linear approximations for determining $Z^2, Z,\ Z^{2/3}$ and $Z^{1/3}$ at different currents have been made, and are presented in table 5.3. The approximations are two-point linear equations and are therefore rough estimations.

Table 5.3 Linear approximations for calculating values of $Z^2, Z,\ Z^{2/3}$ and $Z^{1/3}$ at different stored beam currents in the MAX IV 3 GeV storage ring. I denotes the stored beam current in [mA].

Date	2017-01-26, 2017-01-29
Z^2	$2.98 + 0.0386 \cdot I$
Z	$2.14 + 0.00500 \cdot I$
$Z^{2/3}$	$2.07 + 0.00238 \cdot I$
$Z^{1/3}$	$2.03 + 0.000952 \cdot I$

Since the residual gas is hydrogen-dominated, the low current molecule values of the atomic number become close to that of a pure hydrogen residual gas H_2, which would generate molecule atomic numbers of $Z^2 = 1^2 + 1^2 = 2$, $Z = 1 + 1 = 2$ and $Z^{1/3} = 1^{1/3} + 1^{1/3} = 2$. As seen in tables 5.1 – 5.3, the Z value increases with increasing current. Note that the computed molecule squared residual gas atomic number is not the same as the molecule residual gas number squared, which motives the calculations of $Z,\ Z^{1/3},\ Z^{2/3}$ and Z^2 separately.

5.1.2 Betatron functions

Table 5.4 presents the betatron function values used to calculate transversal acceptances and lifetimes using equations (2.8), (2.20) and (2.22). A MATLAB based LOCO [17] has been used to calculate betatron functions. Design betatron function values are also presented.

Table 5.4 MAX IV 3 GeV betatron function values used to calculate horizontal and vertical acceptances and elastic gas scattering lifetimes for the spring 2017 optics. H1, V2 and V3 301L refer to the horizontal and the lower and upper vertical scrapers located in the first achromat of the MAX IV 3 GeV storage ring.

	$\boldsymbol{\beta_x}$ [m] H1 301L s = 525.94 m	$\boldsymbol{\beta_y}$ [m] V2 301L s = 526.07 m	$\boldsymbol{\beta_y}$ [m] V3 301L s = 526.10 m	$\overline{\boldsymbol{\beta_x}}$ [m]	$\overline{\boldsymbol{\beta_y}}$ [m]
LOCO	9.17 ± 0.12	3.86 ± 0.02	3.79 ± 0.02	3.67 ± 0.06	6.83 ± 0.03
Design	9.48	3.85	3.78	3.73	6.85

LOCO results yield betatron function values along the longitudinal *s*-coordinate around the storage ring. Average betatron function values are the average values for one circumference turn. The errors are estimated values based on previous LOCO fitted betatron function errors [22]. As observed in table 5.4, the LOCO measured betatron function values are close to design.

5.1.3 Beam sizes and emittance

During scraper measurements, the transversal and longitudinal beam sizes have been recorded at the diagnostic beamline. The emittance coupling factor has been calculated by equation (2.3). Table 5.5 details results from measured beam sizes, emittance and coupling factor for the MAX IV 3 GeV storage ring spring 2017 optics.

Table 5.5 Averaged measured beam sizes and emittances during scraper measurements in the MAX IV 3 GeV storage ring. Values are for the spring 2017 production optics, at 70 mA stored beam current. β_x and β_y values refer to the diagnostic beamline radiation source location, and are determined by LOCO measurements. σ_E and η_x are design values.

$\boldsymbol{I}$	70 mA	$\boldsymbol{\beta_x}$	1.21 ± 0.02 m
$\boldsymbol{V_{tot}}$	1.08 MV	$\boldsymbol{\beta_y}$	15.66 ± 0.08 m
$\boldsymbol{\sigma_s}$	1.64 ± 0.04 cm	$\boldsymbol{\varepsilon_x}$	351 ± 19 pm rad
$\boldsymbol{\sigma_x}$	20.9 ± 0.6 μm	$\boldsymbol{\varepsilon_y}$	22 ± 2 pm rad
$\boldsymbol{\sigma_y}$	18.7 ± 0.7 μm	κ	6 %
$\boldsymbol{\sigma_E}$	$7.69 \cdot 10^{-4}$	$\boldsymbol{\eta_x}$	4.1 mm

Beam sizes, bunch-length and emittance errors are population based standard deviations from measurements done during the scraper measurements carried out in April 2017, detailed in section 5.2. The β_x and β_y error magnitudes are estimations based on previous LOCO calculation errors [22]. Emittance errors are taking the error in beam size into account, but omitting the relatively small error in beta-functions.

5.2 Scraper measurements

5.2.1 Horizontal scraper measurements

A horizontal scraper measurement yields a minimum value of the horizontal acceptance. Figure 5.1 illustrates a horizontal scraper measurement located at a non-dispersive s-position in the MAX IV 3 GeV storage ring.

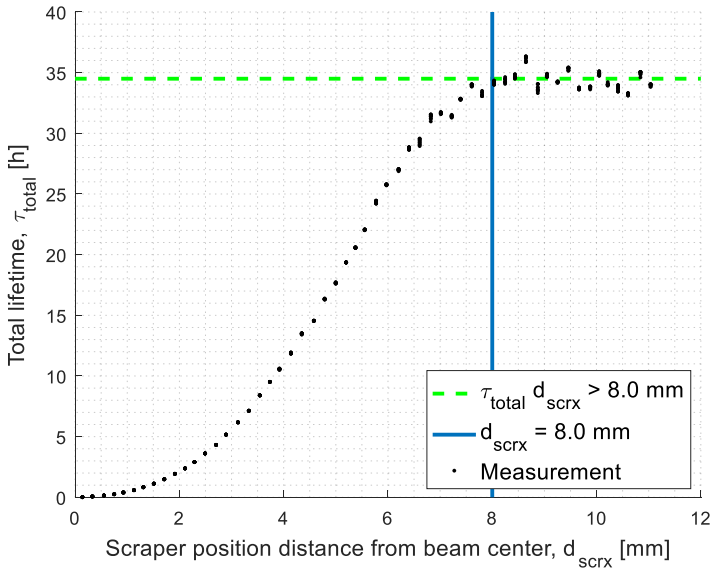

Figure 5.1 Horizontal scraper measurement in the MAX IV 3 GeV storage ring. Black dots show measurements and the blue line illustrates the position where the horizontal scraper has an impact on the total lifetime. The scraper measurement yields a minimum horizontal acceptance.

The measurement in figure 5.1 specifies a minimum value for the horizontal acceptance in the MAX IV 3 GeV storage ring by April 2017, equation (2.8):

$$A_{x\,;\,min} = \frac{8.0^2 \cdot 10^{-6}}{9.17} \approx 7.0 \pm 0.4 \text{ mm mrad.}$$

The error estimation is based on an uncertainty in where the scraper position is affecting the total lifetime of ± 0.2 mm, not taking the error in the beta function value from table 5.5 into account. The minimum required acceptance estimated 2009 was 7.0 mm mrad [23]. In an ideal scenario, where the storage ring would have perfect alignment, the limiting physical horizontal aperture should be given by the septum injection magnet blade, at a 10 mm distance from the beam center [24]. The design value of the horizontal betatron function at this position is $\beta_x = 9.402$ m. A theoretical maximum value of the horizontal physical acceptance is given by:

$$A_{x\,;\,max} = \frac{10.00^2 \cdot 10^{-6}}{9.402} \approx 10.64 \text{ mm mrad.}$$

More horizontal scraper measurements have indicated that the minimum value of the horizontal acceptance is 7.0 mm mrad. A minimum value of $A_x \approx 7.0 \pm 0.4$ mm mrad is therefore confirmed in the MAX IV 3 GeV storage ring by April 2017. Other measurements have shown smaller values of the minimum horizontal acceptance, indicating that the effect on total lifetime seen during the horizontal scraper measurements is due to the scraper blade having an impact on the lattice momentum acceptance, which lowers Touschek lifetime and inelastic scattering lifetimes, rather than the scraper blade affecting the acceptance and elastic scattering lifetime.

Figure 5.2 illustrates the calculated effect that the scraper blade has on the elastic scattering on nuclei lifetime and the other lifetimes. The measurement was performed 170409, at 70 mA stored beam current. The elastic scattering on nuclei lifetime value at the outer scraper position is based on combined horizontal and vertical scraper measurements, detailed in section 5.2.2. The calculated elastic scattering on nuclei lifetime decrease with decreasing horizontal acceptance is formed by equations (2.20) – (2.22), evaluated for a horizontal acceptance of $A_x = 7.00$ mm mrad for $d_{scrx} > 8.00$ mm. $A_x = 7.00$ mm mrad is the minimum horizontal acceptance value for $d_{scrx} > 8.00$ mm, and $d_{scrx} = 8.00$ mm the limiting half-aperture position as measured by the horizontal scraper.

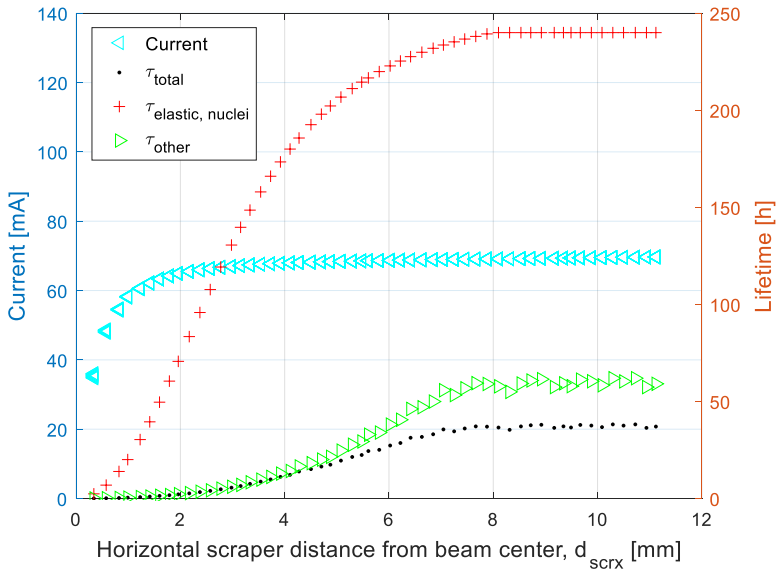

Figure 5.2 Expected elastic scattering on nuclei lifetime decrease versus horizontal scraper position for an assumed minimal horizontal acceptance for $d_{scrx} > 8.00$ mm. The measured total lifetime yields the inverse sum of all other lifetime contributions. The stored beam current during the horizontal scraper measurement is also shown.

5.2.2 Vertical and combined scraper measurements

Vertical scraper measurements have been carried out in the MAX IV 3 GeV storage ring. Each scraper measurement has been analyzed by fitting a model curve to the measurement data, and different lifetimes were separated by the method described in section 4.3.2. This section accounts for the vertical, and combined vertical and horizontal scraper measurement results.

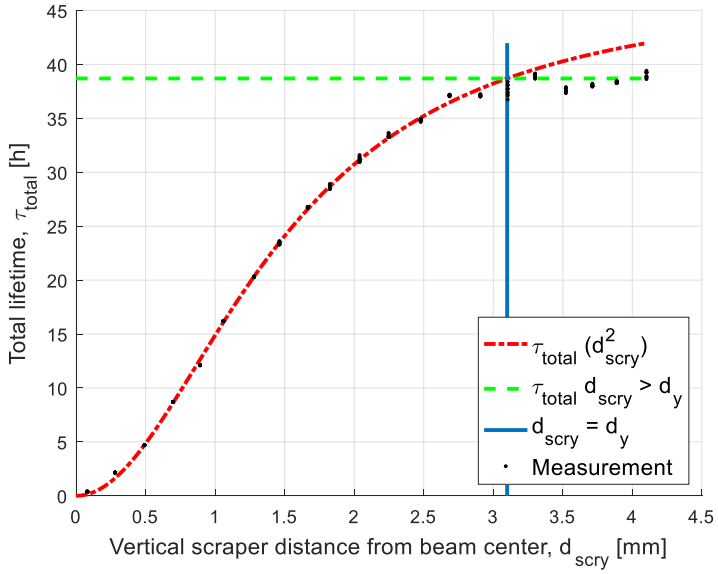

Figure 5.3 Vertical scraper measurement at 70 mA stored beam current. Black dots are the measurements and the red curve the model fit by equation (4.1).

The measurement data and model fit from a single vertical scraper measurement is illustrated in figure 5.3. The vertical scraper measurements give results of the elastic scattering on nuclei lifetime, and other lifetimes as described in methods section 4.3.1 and 4.3.2.

By equation (4.1), the fitted model predicts that the only lifetime affected by the vertical scraper is the elastic scattering on nuclei lifetime. As described in section 4.3.4, Touschek-scattered electrons could be lost against the vertical scraper due to betatron coupling. Scraper measurements carried out prior and during this master's thesis project initially resulted in total gas scattering lifetimes of around 40-70 h, which is considered low. Synchrotron light sources typically have gas scattering lifetimes around and above 100 h [25]. A possible cause of these results was Touschek-scattered electrons being lost against the vertical scraper.

A method to experimentally test if the vertical scraper affects not only the elastic scattering on nuclei lifetime, but also other lifetimes, is to perform two vertical scraper measurements subsequently at different accelerating voltages. The elastic scattering lifetimes should be identical between the two cases, but the Touschek lifetime and inelastic scattering lifetimes should change due to the change in accelerating voltage and RF momentum acceptance, if the RF momentum

acceptance is lowered to such level that it affects the overall momentum acceptance. Figure 5.4 illustrates such a measurement in the MAX IV 3 GeV storage ring. The total lifetime was different for the two cases outside the vertical limiting aperture position, as expected. Yet, as the vertical scraper was moved towards the beam center, the lifetime curves were similar within the limiting aperture position for the two cases. This indicated that the vertical scraper was affecting not only the elastic scattering on nuclei lifetime, but also the other lifetimes.

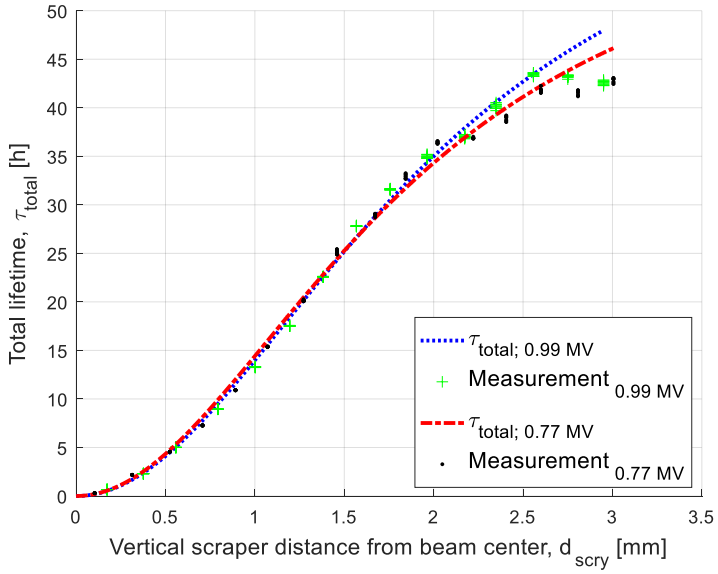

Figure 5.4 Two consecutive vertical scraper measurement at different total accelerating voltages, 0.99 and 0.77 MV respectively, in the MAX IV 3 GeV storage ring. The graph illustrates the measured lifetimes and fitted models for scraper positions less than the vertical limiting aperture distance. The similar measurement data for the two cases indicates that the vertical scraper affects not only elastic scattering on nuclei lifetime, but other lifetime contributions as well.

As described in section 4.3.4, a method to decrease the effect of Touschek-scattered electrons possibly being lost against the vertical scraper is to combine horizontal and vertical scrapers. A series of vertical scraper measurements were performed for different fixed horizontal scraper positions of 8, 6, 5, 4 and 3 mm. The horizontal scraper affects the horizontal acceptance at a minimum distance of 8 mm from the beam center, confirmed by horizontal scraper measurements, results section 5.2.1. Figure 5.5 illustrates three of the five vertical scraper scans, performed at horizontal scraper positions 6, 5 and 4 mm from the beam center.

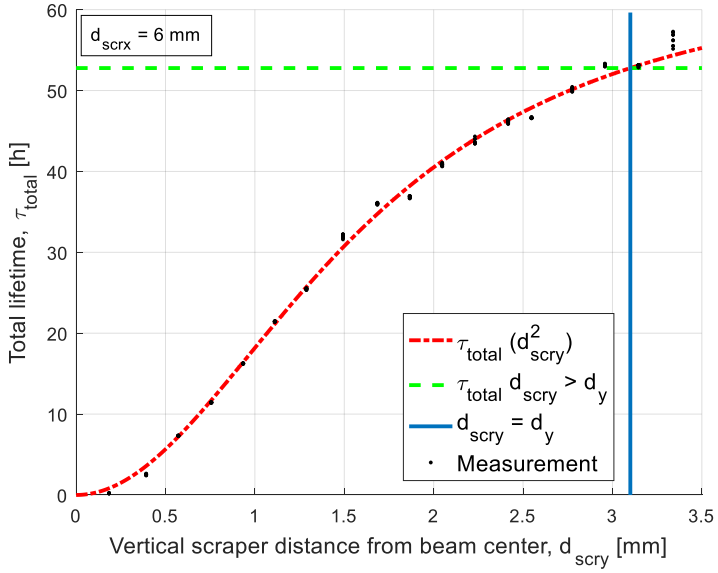
d scrx = 6 mm
Total lifetime, τ total [h]
Vertical scraper distance from beam center, d scry [mm]
τ total (d2 scry)
τ total d scry > d y
d scry = d y
Measurement

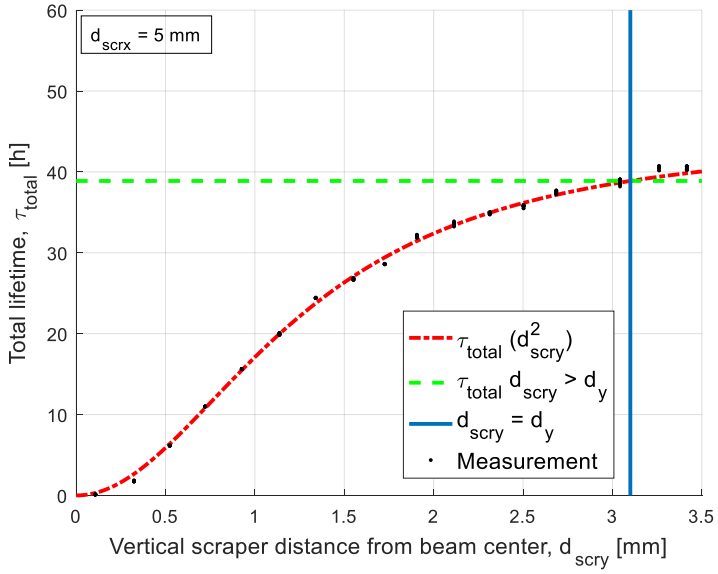
d scrx = 5 mm
Total lifetime, τ total [h]
Vertical scraper distance from beam center, d scry [mm]
τ total (d2 scry)
τ total d scry > d y
d scry = d y
Measurement

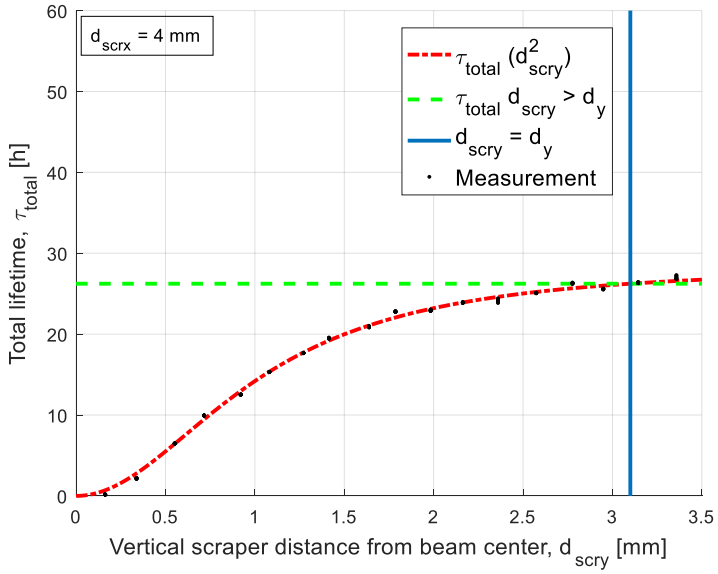
d scrx = 4 mm
Total lifetime, τ total [h]
Vertical scraper distance from beam center, d scry [mm]
τ total (d2 scry)
τ total d scry > d y
d scry = d y
Measurement

Figure 5.5 (*page 36*) MAX IV 3 GeV vertical scraper scans performed at fixed horizontal scraper positions of 6, 5 and 4 mm. The measurements were made at 70 mA stored beam current. Red curves show the model fits by equation (4.1), including the $F(\rho)$ dependence on horizontal and vertical acceptance given by equations (2.21) and (2.22). Text boxes on the upper left indicate the horizontal scraper position distance from the beam center for each scan. $d_y = 3.1$ mm is the limiting vertical half-aperture.

The five measurements resulted in elastic scattering on nuclei lifetimes of 197, 206, 207, 180 and 134 h for 8, 6, 5, 4 and 3 mm fixed horizontal scraper positions respectively. As predicted by the assumption that Touschek-scattered particles could couple to the vertical plane and be lost against the vertical scraper during a vertical scraper measurement, the obtained values of the elastic scattering on nuclei lifetime are expected to be more accurate with decreasing horizontal scraper position from the beam center. Touschek-scattered particles are lost to a smaller degree against the vertical scraper as the horizontal scraper is moved closer to the beam center, as described in methods section 4.3.4.

By comparing calculated values of the expected elastic scattering on nuclei lifetime decrease versus horizontal scraper position with measurements, an increased estimated value of the elastic scattering on nuclei lifetime was obtained, compared to previous vertical scraper measurements. Figure 5.6 illustrates the elastic scattering on nuclei lifetime results obtained from the vertical scraper scans performed at fixed positions of 8, 6, 5, 4 and 3 mm of the horizontal scraper. A calculated curve for an elastic scattering on nuclei lifetime of 240 h is also given, fitted to agree with measurement data.

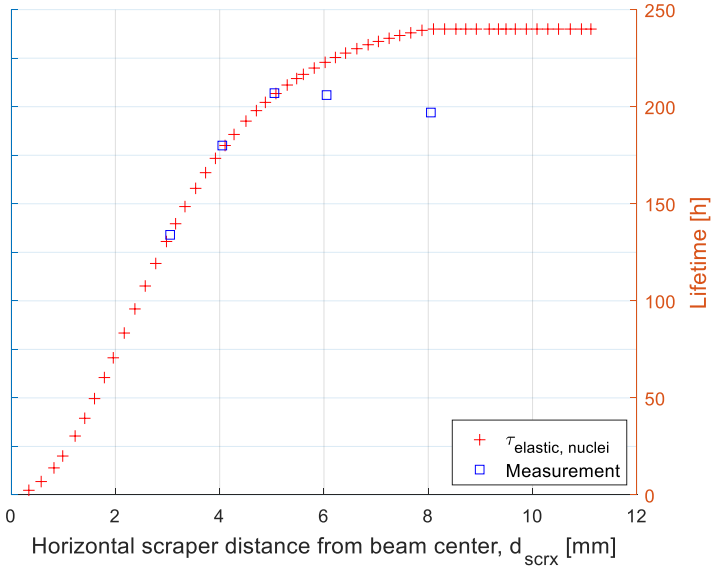

Figure 5.6 MAX IV 3 GeV elastic scattering on nuclei lifetime measurements including a calculated decrease of elastic scattering on nuclei lifetime versus horizontal scraper position. Vertical scraper scans at fixed horizontal scraper positions close to the beam center decrease the effect of Touschek-scattered particles being lost against the vertical scraper due to betatron coupling, possibly yielding low results of the elastic scattering on nuclei lifetime from a vertical scraper measurement.

The red curve for figure 5.6 is fitted against measurement data, assuming that the measurements are more accurate the closer the horizontal scraper is to the beam center. The vertical acceptance used in the calculation is 2.5 mm mrad, as estimated by vertical scraper measurements, results section 5.2.3. The fitted curve in figure 5.6 indicates that the elastic scattering on nuclei lifetime is approximately 240 h with an error of ± 24 h. The error is equal to the population standard deviation of 10 measured elastic scattering on nuclei lifetime results from April 2017. All measurements are made for the spring 2017 optics, at 1.08 MV accelerating voltage, 70 mA stored beam current and even bunch populated filling pattern.

The result from the combined horizontal and vertical scraper measurements is expected to improve the estimation of elastic scattering on nuclei lifetime. The estimation of the elastic scattering on nuclei lifetime of 240 h from the combined horizontal and vertical scraper scans was used as a reference for other vertical scraper measurements carried out in April 2017. The presumption that the elastic scattering lifetime is unchanged during April 2017 is based on no observed pressure change between the measurements. All measurements are carried out at the same storage ring optics. Figure 5.7 illustrates a vertical scraper measurement.

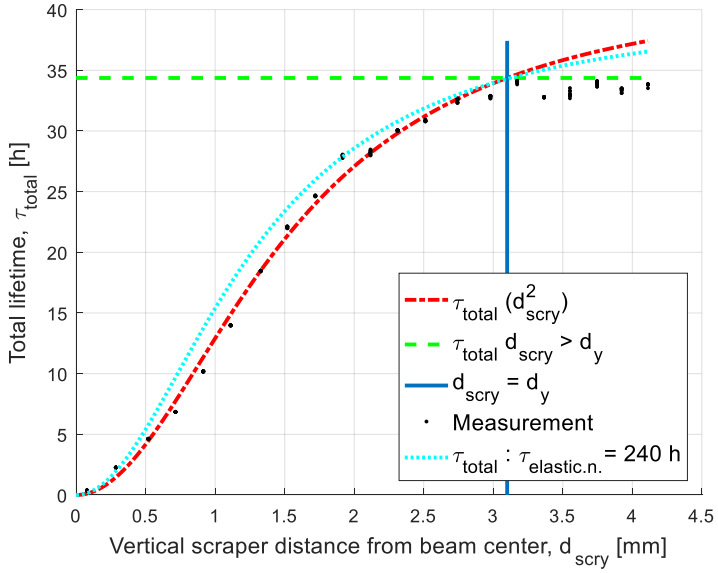

Figure 5.7 Vertical scraper measurement in the MAX IV 3 GeV storage ring at 70 mA stored beam current. The cyan curve illustrates the expected curve shape for an elastic scattering lifetime of 240 h, as estimated by combined horizontal and vertical scraper measurements from the same period. The cyan curve illustrates the possible case were no Touschek-scattered electrons are lost against the vertical scraper due to betatron coupling.

During the measurement in figure 5.7, the vertical scraper likely affected Touschek-lifetime. The dashed cyan curve illustrates the expected lifetime dependence on scraper position if the scraper would only have impacted the elastic scattering on nuclei lifetime, if the elastic scattering on nuclei lifetime would have agreed with the results obtained by the combined horizontal and vertical scraper measurements. This illustrates the expected result in a low betatron-coupled optics, where Touschek-scattered particles only are lost against the limiting vertical aperture to a small degree.

Figure 5.8 illustrates two MAX IV 3 GeV vertical scraper measurements. One measurement was performed with the lower vertical scraper, and one with the upper. Measurements were made subsequently. Negative distance from the beam center illustrates the lower scraper position from the center.

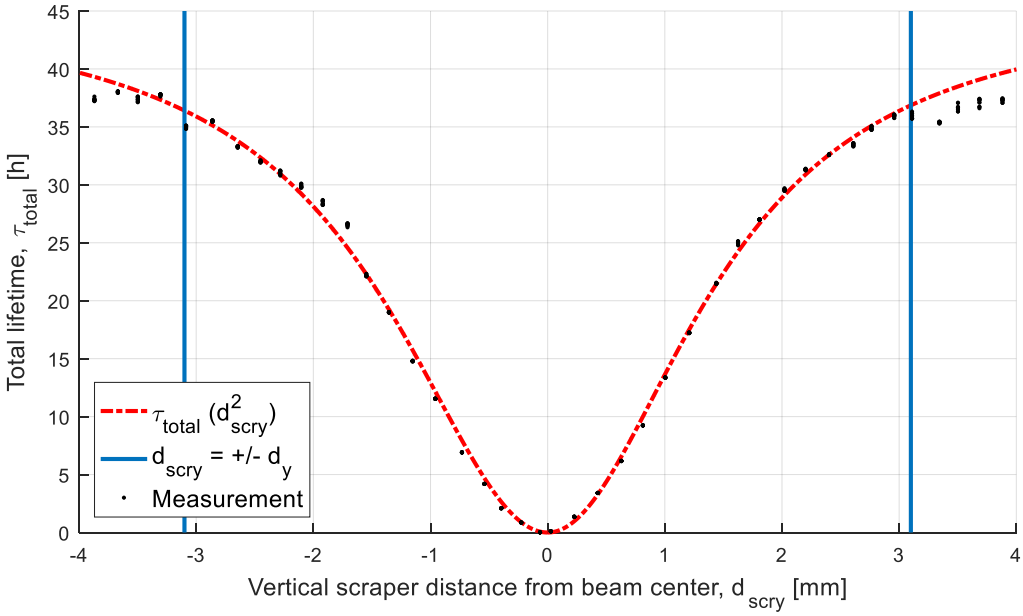

Figure 5.8 MAX IV 3 GeV vertical scraper measurements. The graph illustrates two separate scraper measurements, one performed with the lower vertical scraper and one with the upper. The measurements were made at 70 mA stored beam current for the spring 2017 production optics, 1.08 MV accelerating voltage and an evenly populated bunch pattern. The red line is the fitted model curve.

5.2.3 Vertical acceptance

The vertical acceptance has been estimated by vertical scraper measurements. Results yields a vertical acceptance in the MAX IV 3 GeV storage ring by April 2017, equation (2.8):

$$A_y \approx \frac{3.1^2 \cdot 10^{-6}}{3.86} \approx 2.5 \pm 0.2 \text{ mm mrad.}$$

The uncertainty takes the scraper position impact point on the total lifetime uncertainty of ± 0.2 mm into account, but omits the uncertainty in the beta-function value specified in table 5.4. The minimum required vertical acceptance estimated 2009 was 1.3 mm mrad [23]. The current theoretical maximum physical acceptance limit is given by in-vacuum insertion devices and is $A_{y;max} \approx 4.0$ mm mrad [21].

5.2.4 Lifetimes

This section presents the obtained lifetimes for the MAX IV 3 GeV storage ring production optics by May 2017. The results are calculated using fitted models to horizontal and vertical scraper measurement data described in section 5.2.2. Data from rest gas analyzers and MATLAB LOCO measurements are also used in the calculations.

Table 5.6 MAX IV 3 GeV storage ring lifetimes derived by scraper measurements. The lifetimes are given for the spring 2017 production optics, 70 mA even bunch populated filling pattern and a total accelerating voltage of 1.08 MV.

		$\tau_{elastic\ nuclei}$	240 ± 24 h
I	70 mA	$\tau_{elastic\ electrons}$	11100 ± 700 h
V_{tot}	1.08 MV	$\tau_{inelastic\ nuclei}$	255 ± 15 h
f_{RF}	99.930 845 860 MHz	$\tau_{inelastic\ electrons}$	451 ± 27 h
κ	6 %	τ_{gas}	96 ± 4 h
τ_{total}	36 ± 3 h	$\tau_{Touschek}$	59 ± 7 h

The results of the elastic scattering on nuclei lifetime is based on the fitted curve to the results of the combined horizontal and vertical scraper scans from 2017-04-26, illustrated in figure 5.6. The error is based on the population standard deviation of 10 vertical scraper elastic scattering on nuclei results from April 2017. All other lifetimes are results from 10 upper and lower vertical scraper scans performed at 70 mA during April 2017, where the elastic scattering on nuclei lifetime has been presumed to agree with the result obtained 2017-04-26. Error estimations do not account for the possible error in Z, or the beta-function errors presented in table 5.4. The error in the elastic scattering lifetime is not considered, hence the presented errors originate from the total lifetime variation for an elastic scattering on nuclei lifetime of 240 h.

Several scraper measurements have been performed prior and during this thesis project, at varied optics settings, accelerating voltages and currents. This is due to the MAX IV 3 GeV storage ring being in its early stage of operation, with beamline commissioning ongoing. The results presented in table 5.6 are all made at the same optics, accelerating voltages and currents. A bunch-by-bunch feedback system was active during all measurements, keeping the energy spread σ_E constant.

Expected lifetimes from 2009 can be found in references [23]. Expected lifetimes are given for 500 mA stored beam current, and both gas scattering and Touschek scattering lifetimes are current dependent. For the gas scattering lifetime, the measured product of current and lifetime can be compared to the target. The measured product is $70\ \text{mA} \cdot 94\ \text{h} \approx 7\ \text{Ah}$ and the target is $500\ \text{mA} \cdot 20\ \text{h} = 10\ \text{Ah}$. The gas scattering lifetime is expected to increase with time and integrated current dose, due to continuous conditioning of the vacuum chambers.

For the Touschek lifetime result, it must be considered that measurements during the work of this thesis project has not been using passive Landau cavities in the storage ring, which are expected to stretch the electron bunch length to a factor 5 times the natural bunch length. As described in section 2.2.4, the Touschek lifetime scales proportional to the rms bunch length σ_s. Yet, measured bunch lengths in table 5.5 are a factor 1.4 times the natural bunch length. This factor can be explained by potential well distortion [21]. How strong this effect will be is unknown for the case with stretched bunch lengths using Landau cavities, but is not believed to

increase [21]. This leaves an interval approximation for the measured Touschek lifetime scaled to 500 mA, with passive Landau-cavities in operation. The Touschek scattering lifetime of 59 h measured by scrapers presented in table 5.6 would range in the interval $70/500 \cdot 5 \cdot \sqrt{0.024}/\sqrt{0.06} \cdot 59/1.4 \approx 18.7$ h to $18.7 \cdot 1.4 \approx 26.1$ h accounting for 500 mA stored beam current and stretched bunch-lengths using passive Landau cavities. The factors under square root signs are considering the measured coupling factor versus the design coupling factor. A Touschek lifetime estimate by 2009 for 500 mA current, with Landau cavities was 25.5 h [23]. Also, at the time of writing, May 2017, projects to optimize the lattice momentum acceptance, and with it the overall momentum acceptance, of the storage ring has not yet been started. The estimated overall momentum acceptance for the spring 2017 optics is 3.9 ± 0.1% at 1.08 MV total accelerating voltage, results section 5.3.1. Increased momentum acceptance will improve the Touschek lifetime, by equation (2.26). Taking this into account, the measured interval result of 18.7-26.1 h, which is scaled for 500 mA using Landau cavities, is close to the 2009 target value of 25.5 h.

5.2.5 Pressure seen by the electron beam

The elastic scattering on nuclei lifetime reveals the average pressure seen by the electron beam by equation (2.20). This pressure might differ from the average pressures recorded by ion pumps or vacuum gauges. As described by Wiedemann [3], the averaged betatron function value found in the equation for the elastic scattering on nuclei lifetime is an approximation for the limit of the maximum allowed scattering angle. The pressure gives the probability of Coulomb scattering, and the amplitude of the betatron function at the scattering location yields the effect of the scattering [3]. Hence, locally high pressures at high betatron function amplitudes would reveal an averaged higher pressure seen by the electron beam, than the actual average pressure of the entire storage ring.

The pressure calculated by equation (2.20) depends on the estimated molecule atomic number of the residual gas. Storage rings with low Z-values of the residual gas, as the MAX IV 3 GeV storage ring, can reveal high vacuum pressure seen by the electron beam and still yield high gas scattering lifetimes. For a hydrogen dominated residual gas, the effect of Coulomb scattering on the nuclei is low. Table 5.7 displays the average pressure recorded from scraper measurements performed during late spring 2017, for a stored beam current of 70 mA. Average pressure from ion pumps and estimated vacuum gauge pressure values are also accounted for.

Table 5.7 Average pressures in the MAX IV 3 GeV storage ring as measured in April 2017. P_{scr} denotes the average pressure seen by the electron beam as calculated by scraper measurements, P_{ion} is the pressure measured by the ion pumps and P_{vg} is the expected average pressure as measured by vacuum gauges based on a linear approximation [20]. All pressures are given for 70 mA stored beam current.

$\boldsymbol{I}$	70 mA
$\boldsymbol{P_{scr}}$	$6.68 \pm 0.04 \cdot 10^{-9}$ mbar
$\boldsymbol{P_{ion}}$	$1.44 \pm 0.03 \cdot 10^{-8}$ mbar
$\boldsymbol{P_{vg}}$	$5.25 \cdot 10^{-10}$ mbar

The scraper measurement pressures are calculated from the results in table 5.6, where elastic scattering lifetimes are taken to be 240 h, as measured in April 2017. The error in pressure from scraper measurements originates from the difference in measured acceptances from the measurements. The error in pressure from ion pumps is the population standard deviation. As seen in table 5.7, the pressure seen by the electron beam calculated from scraper measurements is roughly one order of magnitude higher than the 70 mA approximated value from the vacuum gauges. The ion pumps show a higher average pressure than the pressure calculated by scrapers. Ion pumps have been suspected to show too high average pressure values, due to emitted photoelectrons increasing the ion pump currents [21]. This is also indicated by the scraper measurements. For both vacuum gauges and ion pumps, it must be considered that these do not measure the pressure in the beam location, but locally around the storage ring. This is also true for rest gas analyzers. If the beam would see a different residual gas molecule Z than the RGA's, the average pressure estimated by scrapers will change according to equation (2.20).

5.3 Momentum acceptance

5.3.1 OPA overall momentum acceptance estimations

The storage ring local momentum acceptance is the minimum value of the RF momentum acceptance and the lattice momentum acceptance along the longitudinal coordinate of the storage ring. The overall momentum acceptance, which is the local momentum acceptance averaged over all s-coordinates, has been estimated using OPA [8]. By calculating expected Touschek lifetimes based on emittance coupling, total accelerating voltage and longitudinal bunch-length and compare with measured Touschek lifetimes, an estimation of the overall momentum acceptance has been made. This section details the results from such simulations.

Measured Touschek lifetimes are 59 ± 7 h from table 5.6, given for a total accelerating voltage of 1.08 MV. The RF momentum acceptance for this accelerating voltage is 4.7%, by equation (2.9). Yet, Touschek lifetimes simulated by OPA are 135 h for $E = 3.0\ \text{GeV},\ \kappa = 6\%,\ V_{tot} = 1.08\ \text{MV},$ $I = 70\ \text{mA}$, scaled for $\sigma_s = 1.65\ \text{cm}$, at an even populated bunch filling pattern. The overall

momentum acceptance is limited by the RF in the OPA simulations. By equation (2.26), the local momentum acceptance influences the Touschek lifetime, which leads to the conclusion that the storage ring overall momentum acceptance is limited by the lattice momentum acceptance, and not the RF momentum acceptance. By alternating the total accelerating voltage in OPA, and scaling the obtained natural bunch lengths for $\sigma_s = 1.65$ cm so that simulated Touschek lifetimes agree with measurements, the lattice momentum acceptance has been estimated. The result is presented in table 5.8.

Table 5.8 Measured parameters including the OPA estimated overall momentum acceptance for the spring 2017 production optics of the MAX IV 3 GeV storage ring.

		κ	6 %
I	70 mA	σ_s	1.64 ± 0.04 cm
V_{tot}	1.08 MV	τ_{total}	36 ± 3 h
f_{RF}	99.930 845 860 MHz	τ_{gas}	96 ± 4 h
ϵ_{acc}	3.9 ± 0.1%	$\tau_{Touschek}$	59 ± 7 h

The result is an estimated overall momentum acceptance of $\epsilon_{acc} \approx 3.9 \pm 0.1\%$, which generates Touschek lifetimes between 53 and 68 h, taking the uncertainty into account. The result is considered reasonable, since projects to optimize the lattice momentum acceptance have not been started yet. The minimum required overall momentum acceptance estimation 2009 was 4.5% [23].

5.4 Current decay

5.4.1 Stored beam decay

Described in section 2.2, different lifetimes give rise to different current decay processes. Figure 2.5 illustrates diverse types of decays. In this section, lifetimes obtained from scraper measurements are used to compare measured current decays with model calculated decays, and the results are discussed. Figure 5.9 illustrates measured and model calculated current decays and lifetimes from 170413.

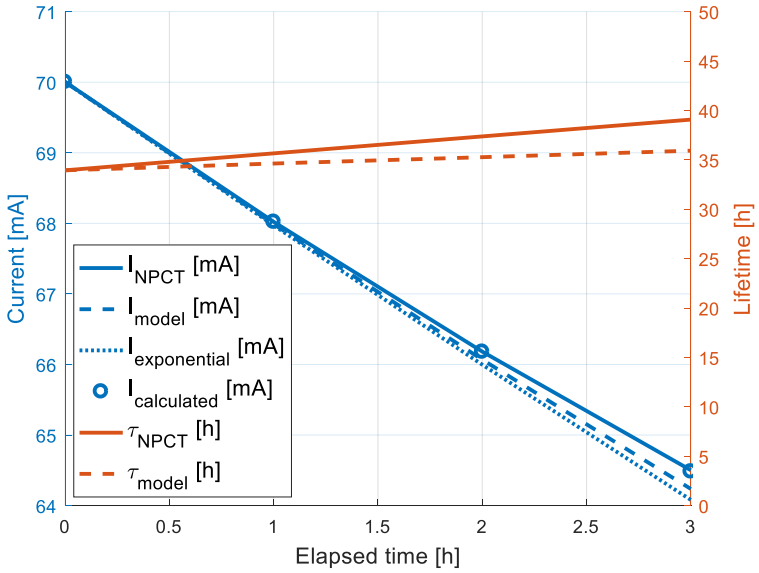

Figure 5.9 MAX IV 3 GeV storage ring current decay (left axis) and lifetime increase (right axis) over time from 00:10:38 to 03:10:38 on 170413. NPCT recorded stored beam current decay and lifetime increase is compared to the model decays using scraper measurement results and equation (2.17). A pure exponential decay is also illustrated, as well as a calculated current decay confirming that the lifetime determined by the NPCT is adequate.

Based on results from scraper measurements 170412, a total lifetime of 33.9 h results in a gas scattering lifetime of 83.4 h and a Touschek scattering lifetime of 57.2 h. To first approximation, where the storage ring pressure is not dependent on the current, the gas scattering lifetime gives rise to an exponential decay, and the Touschek lifetime generates a hyperbolic decay. The calculated current decay and lifetime increase based on the model by equation (2.17) are illustrated in figure 5.9, denoted by model in the index. Together with these model values, also the NPCT recorded current decay and lifetime increase are illustrated. A pure exponential decay is also given, denoted by exponential in the index. Finally, a calculated current decay using equation (2.17) and the lifetime increase recorded by the NPCT is made, illustrated by the circle points. The calculated decay points coincide with the NPCT recorded current decay graph, as expected, and verifies that the software based lifetime calculation made by the NPCT is correct.

However, the pressure is not constant with current but increases with increasing current due to synchrotron radiation hitting the inside of the vacuum chambers, increasing the pressure with increasing current. This current dependent pressure which affects elastic and inelastic scattering lifetimes gives rise to a hyperbolic decay, while the base pressure, which remains constant, creates an exponential decay. Approximately, the pressure increases linearly with current, $P_{total} = P_{base} + P_{eff} \cdot I$. Taking this into account would bring I_{model} slightly closer to I_{NPCT} in figure 5.4, but the effect is considered minor since the current decrease is only about 5.5 mA or 7.86% of the starting current I_0.

It shows that the product of current and lifetime, $I \cdot \tau$, increases with decreasing current. This cannot be explained even by letting all lifetime contributions in the example generate a hyperbolic current decay, which would be the case when $P_{base} = 0$. This would keep the product of current and lifetime constant, which is the characteristic property of a hyperbolic decay. A few causes could explain the increase of $I \cdot \tau$ over time, which has been observed not only 170413, but at several occasions during this master's thesis project.

One theory, which needs further investigation, is that the result could be connected to the observed Z-dependence with current. Since different lifetime contributions include dependencies on $Z^{1/3}, Z^{2/3}, Z$ and Z^2, the variation of Z with current could give rise to a current decay which is neither exponential nor hyperbolic, resulting in an increase of the product of current and lifetime over time. This effect could partly, or fully, explain the observed $I \cdot \tau$ increase with time. Another explanation could be that the accelerating voltage increases with decreasing current, increasing overall momentum acceptance and Touschek lifetime. This is unlikely, since OPA simulations indicate that the overall momentum acceptance is limited by the lattice momentum acceptance and not the RF momentum acceptance. Also, the low-level RF system is designed to keep the accelerating voltage constant, by measuring the electric fields in the cavities and regulating the forward power from the RF transmitters.

However, the calculated current decay using the combined exponential and hyperbolic functions by equation (2.17) yields a current loss with time that is closer to the actual monitored current decay than a pure exponential decay. Also, plans to calculate the lifetime based on sum signals from BPM's (beam position monitors) are mentioned [21], which possibly could yield more accurate values of the lifetime. This might render different results.

6. Conclusions

In this work, the lifetime of the MAX IV 3 GeV storage ring has been characterized. The first estimates of the MAX IV 3 GeV Touschek- and gas scattering lifetimes have been obtained from measurements using storage ring scrapers. By combining scraper measurements with betatron function measurements, rest gas analyzer data, transversal beam size measurements and longitudinal bunch length measurements, a vast amount of information has been obtained. Apart from Touschek- and gas scattering lifetimes, estimates of the overall momentum acceptance and the effective pressure seen by the electron beam have been made.

Combined horizontal and vertical scraper scans can give a better estimate of the elastic scattering on nuclei lifetime. Betatron coupling may cause Touschek-scattered particles to be lost against the vertical scraper during vertical scraper scans. Vertical scraper scans at fixed positions of the horizontal scraper are recommended for future lifetime measurements using scrapers.

The overall momentum acceptance has been shown to be limited by the lattice. As beam optics projects to maximize lattice momentum acceptance are started, continued scraper measurements are recommended as a diagnostic tool for the expected improved lifetimes. Furthermore, when optics with a coupling factor closer to design are being developed, scraper measurements could be used to verify the supposed decrease in Touschek lifetime.

The combined exponential and hyperbolic current loss model was not able to fully describe the monitored current loss observed in the MAX IV 3 GeV storage ring. However, it illustrated a current decay that was closer to the monitored than a pure exponential decay. An increase of the current and lifetime product with time was observed. This effect cannot be explained even by a pure hyperbolic decay. A theory of the observed residual gas Z average atomic number decrease with decreasing current affecting the separate lifetimes as the cause of the increase of the current and lifetime product with time has been suggested, and needs further investigation.

When performing studies at a synchrotron, to keep extreme caution and closely observe and note parameters during measurements could not be emphasized enough. Synchrotrons are complex machines, where observed phenomena can have close to infinitely many root causes. The author was advised this before the project started, and now realizes the importance of this fact. The advice is passed on further.

An ideal scenario when performing measurements using storage ring scrapers in a synchrotron would be a finalized production optics for the storage ring. The MAX IV 3 GeV storage ring is still in its early stage of operation. Non-linear optics projects, which would result in increased overall momentum acceptance, have not been started yet. The work carried out during this thesis project are initial beam dynamics studies, to be continued as the MAX IV project continues.

References

[1] Å. Andersson *et al.*, "Diagnostics at the MAX IV 3 GeV Storage Ring during Commissioning," in *IBIC 2016*, Barcelona, Spain, 2016.

[2] S. C. Leemann, M. Sjöström, and Å. Andersson, "First optics and Beam Dynamics Studies in the MAX IV 3 GeV Storage Ring," in *IPAC'17*, Copenhagen, Denmark, 2017, no. WEPAB075.

[3] H. Wiedemann, *Particle Accelerator Physics*. Berlin Heidelberg: Springer-Verlag, 2007.

[4] K. Wille, *The Physics of Particle Accelerators, an introduction*. New York: Oxford University Press Inc., 2005.

[5] P. Willmott, *An Introduction to Synchrotron Radiation: Techniques and Applications*. West Sussex: John Wiley & Sons, Ltd, 2011.

[6] A. L. Robinson, "History of Synchrotron Radiation," *Synchrotron Radiation News,* vol. 28:4, pp. 4-9, 2015.

[7] A. Streun, "Momentum Acceptance and Touschek lifetime," *SLS Note,* vol. 18/97, 1997 corr. 2008.

[8] A. Streun, "OPA Lattice Design Code," 3.59 ed. Swiss Light Source (SLS), 2012.

[9] A. Hansson, "Electron beam sizes and lifetimes at MAX II and MAX III," Doctoral, MAX IV Laboratory, Lund University, 2012.

[10] Å. Andersson and A. Streun, "Lifetime and acceptance of the SLS storage ring," in *Proceedings of EPAC*, Edinburgh, Scotland, 2006.

[11] J. L. Duff, "Current and current density limitations in existing electron storage rings," *Nuclear Instruments and Methods in Physics Research,* no. A239, pp. 83-101, 1985.

[12] J. Murphy, *Synchrotron Light Source Data Book*. 1989.

[13] A. Wruhlich, "Single beam lifetime," presented at the CAS - CERN Accelerator School : 5th General Accelerator Physics Course, Jyväskylä, Finland, 1992.

[14] S. C. Leemann, "Lattice Design for the MAX IV Storage Rings," 2016.

[15] P. F. Tavares, S. C. Leemann, M. Sjöström, and Å. Andersson, "The MAX IV storage ring project," *Journal of Synchrotron Radiation,* 19 May 2014.

[16] D. Olsson, "Design of Stripline Kicker for Tune Measurements in the MAX IV 3GeV Ring," in *Progress In Electromagnetics Research Symposium Proceedings*, Stockholm, 2013.

[17] J. Safranek, G. Portmann, and A. Terebilo, "MatLab-based LOCO," in "SLAC-PUB-9464," Stanford, Berkeley, USA, 2002.

[18] J. Breunlin, "Emittance Related Topics for Fourth Generation Storage Ring Light Sources," Doctoral, Lund University, 2016.

[19] J. Breunlin and Å. Andersson, "Emittance diagnostics at the MAX IV 3 GeV storage ring," in *IPAC 2016*, Busan, Korea, 2016.

[20] M. Grabski and E. A. Dmour, Vacuum engineering unit, MAX IV Laboratory, Private communication, 2017.

[21] Å. Andersson, Group manager accelerator physics group, MAX IV Laboratory, Private communication, 2017.

[22] M. Sjöström, "MAX IV Ring Status," ESLS XXIV, 2016.

[23] S.C. Leemann, Å. Andersson, M. Eriksson, L.-J. Lindgren, and E. Wallén, "Beam dynamics and expected performance of Sweden's new storage-ring light source: MAX IV," *Physical Review Special Topics - Accelerators and Beams,* 2009.

[24] S. C. Leemann, "Pulsed sextupole injection for Sweden's new light source MAX IV," *Phys. Rev. ST Accel. Beams,* vol. 15, no. 5, p. 050705, 2012.

[25] U. Iriso, Beam Physics Section Head, Accelerator Division Alba Synchrotron Light Source, Private communication, 2017.